Journal of Biomolecular Structure and Dynamics

ISSN: 0739-1102 (Print) 1538-0254 (Online) Journal homepage: www.tandfonline.com/journals/tbsd20

Synthesis, characterization, molecular docking and molecular dynamics simulations of novel 2,5-disubstituted-1,3,4-thiadiazole derivatives as potential cholinesterase/monoamine oxidase dual inhibitors for Alzheimer's disease

Amal A. AL-Sharabi, Asaf Evrim Evren, Begüm Nurpelin Sağlık & Leyla Yurttaş

To cite this article: Amal A. AL-Sharabi, Asaf Evrim Evren, Begüm Nurpelin Sağlık & Leyla Yurttaş (2024) Synthesis, characterization, molecular docking and molecular dynamics simulations of novel 2,5-disubstituted-1,3,4-thiadiazole derivatives as potential cholinesterase/monoamine oxidase dual inhibitors for Alzheimer's disease, Journal of Biomolecular Structure and Dynamics, 42:23, 13023-13041, DOI: 10.1080/07391102.2023.2274967

To link to this article: https://doi.org/10.1080/07391102.2023.2274967

JOURNAL OF BIOMOLECULAR STRUCTURE AND DYNAMICS
2024, VOL. 42, NO. 23, 13023–13041
https://doi.org/10.1080/07391102.2023.2274967

Synthesis, characterization, molecular docking and molecular dynamics simulations of novel 2,5-disubstituted-1,3,4-thiadiazole derivatives as potential cholinesterase/monoamine oxidase dual inhibitors for Alzheimer's disease

Amal A. AL-Sharabi[a], Asaf Evrim Evren[a,b], Begüm Nurpelin Sağlık[a] and Leyla Yurttaş[a]

[a]Faculty of Pharmacy, Department of Pharmaceutical Chemistry, Anadolu University, Eskişehir, Turkey; [b]Vocational School of Health Services, Department of Pharmacy Services, Bilecik Seyh Edebali UniversityTurkey

Communicated by Ramaswamy H. Sarma

ABSTRACT

Designing multi-targeted drugs (MTD) for Alzheimer's disease (AD) is now one of the priorities for medicinal chemists, as the disease has a complicated not fully understood pathological nature and the approved mono-targeted drugs only alleviate the symptoms. In this study, the synthesis, spectral analyses and *in vitro* inhibition activity against cholinesterase (ChE) and monoamine oxidase (MAO) enzymes of a novel series of *N*-[5-(adamantan-1-yl)-1,3,4-thiadiazol-2-yl]-2-(4-un/substituted) cyclic secondary amino-acetamide/propanamide derivatives were done. Generally, derivatives were more selective against acetylcholinesterase (AChE) and *h*-MAO-B than butyrylcholinesterase (BChE) and *h*-MAO-A, respectively. Derivatives **4a**, **4b**, **3a**, **3d** and **3b** ordered from the most potent to the least displayed significant inhibition against AChE. Also, derivatives **4a**, **4b** and **3a** still maintained their significant inhibition against *h*-MAO-B in the same potency order, making them dual inhibitors and MTD candidates for AD. Binding interactions with several crucial amino acid residues for activity and selectivity as well as the stability of the most active derivatives-enzyme complex were confirmed utilizing molecular docking and molecular dynamic simulation studies.

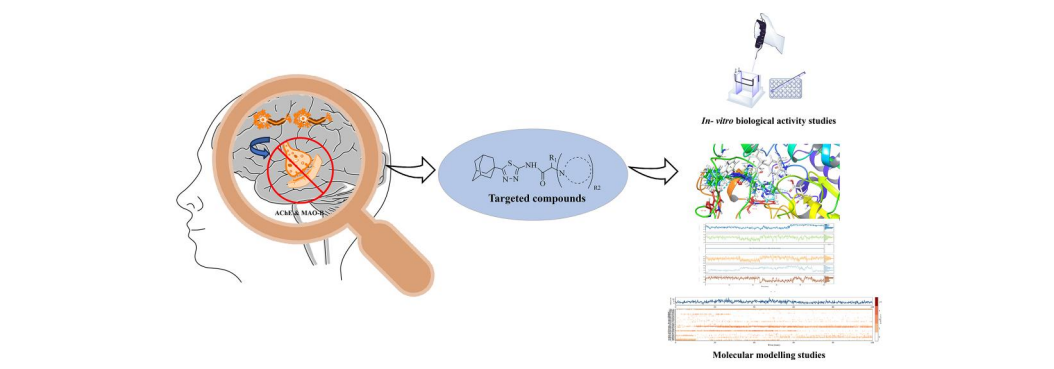

HIGHLIGHTS

- Novel 2,5-disubstituted-1,3,4-thiadiazole derivatives were synthesized.
- The ChEs/MAOs dual inhibition activity against Alzheimer's disease was tested.
- Compounds **4a**, **4b** and **3a** were active dual inhibitor against both AChE and *h*-MAO-B.
- Compounds **3d** and **3b** were also active against AChE.
- No significant inhibition activity against BChE and *h*-MAO-A.

ARTICLE HISTORY
Received 27 March 2023
Accepted 18 October 2023

KEYWORDS
Alzheimer's disease; 1; 3; 4-Thiadiazole; adamantane; acetylcholinesterase inhibitor; monoamine oxidase-B inhibitor; molecular docking; molecular dynamic simulation

Introduction

Alzheimer's disease (AD) is an irreversible progressive neurodegenerative brain disorder that mainly affects the elderly. It is the most common form of dementia which is considered the seventh major cause of death worldwide, with over 55 million cases that are estimated to increase to 78 million by 2030 (Gauthier et al., 2021; World Health Organization, 2021). The most common symptoms related to AD include memory loss, thinking difficulties, poor judgment, difficulty performingdaily familiar tasks, social withdrawal and mood changes. The exact pathological mechanism of AD is not fully understood, however many brain change markers have been

CONTACT Amal A. AL-Sharabi amal_anfa@anadolu.edu.tr Faculty of Pharmacy, Department of Pharmaceutical Chemistry, Anadolu University, 26470, Eskişehir, Turkey.

Supplemental data for this article can be accessed online at https://doi.org/10.1080/07391102.2023.2274967.

observed in patients including neuronal loss, cerebral cortical atrophy, extraneuronal deposition of senile plaques (SPs) with a central core of amyloid-beta (Aβ) aggregates, intraneuronal deposition of neurofibrillary tangles (NFT), overactivation of MAOs, overactivation of *N*-methyl-D-aspartate (NMDA) receptors, dysregulation of metal ions, oxidative stress, neuroinflammation as well as disruption of neurotransmitters systems, mostprominently cholinergic depletion (Abeysinghe et al., 2020; Kumar et al., 2022).

As the cholinergic pathway was noticed to be irreversibly destroyed in the central nervous system of AD patients and the level of acetylcholine (ACh), which is crucial for memory, learning and many other physiological processes, is consequently decreased, inhibiting AChE and BChE which are both types of cholinesterase enzymes that are responsible for the normal degradation of ACh will eventually increase the concentration of the neurotransmitter in the brain of AD patients (Bartus et al., 1982; Marucci et al., 2021). Besides that, MAO enzymes were found to be overexpressed and overactivated in AD patients, especially the isoform MAO-B. This overactivation negatively affects the progression of AD as the concentration of the neurotoxic by-products, including hydrogen peroxides and reactive oxygen species (ROS), increases, leading to exaggerated neuroinflammation, oxidative stress, Aβ deposition, neuronal damage and neuronal death, thus inhibiting MAOs has a neuroprotective effect and is being invistigated as a potential treatment for AD (Guzior et al., 2015; Manzoor and Hoda, 2020).

So far, only six medications have received FDA approval for clinical use in AD (Figure 1). Among these drugs, cholinesterase enzyme inhibitors (ChEIs) include tacrine, donepezil, rivastigmine and galantamine ; however, tacrine has been withdrawn from the market due to hepatotoxicity (Sharma et al., 2019). The other two drugs are memantine as an NMDA receptor antagonist aducanumab as an anti-amyloid monoclonal antibody that was recently approved (2021) (Ferris, 2003; Haddad et al., 2022). Unfortunately, due to the complex nature of AD, none of these drugs, whether used as monotherapy or as combinational therapy, were able to cure or halt the progression of the disease and they only provide symptomatic treatment. Thus, the trend now is shifting toward the development of MTDs that can act on more than one pathological target that are involved in the progression of AD (Kumar et al., 2022; Massoud and Leger, 2011).

In addition to three of the four ChEI drugs with AD licenses that contain heterocyclic systems, heterocyclic compounds have also been widely investigated as AD treatment (Hiremathad and Piemontese, 2017; Martorana et al., 2016). The promising features of the five-membered heterocyclic ring 1,3,4-thiadiazole have been employed for the design and synthesis of many active compounds as it has a wide spectrum of biological activity (Aliabadi, 2016; Jain et al., 2013; Joseph et al., 2015). Several market-available drugs have this moiety including the antibacterial cefazolin sodium and cefazedone, the antiparasitic megazole, and the carbonic anhydrase inhibitor diuretics acetazolamide and methazolamide as shown in Figure 2 (Dawood and Farghaly, 2017; Li et al., 2013). This diversity in the activity is attributed back to the presence of the –N = C–S– group and its ability to be a bio-isostere to many other heterocycles such as oxadiazole, pyridazine and thiazole (Han et al., 2021). Moreover, the mesoionic nature of the ring and the presence of the sulfur atom enhance the lipophilicity, bioavailability as well as blood–brain barrier (BBB) permeability for centrally acting drugs (Haider et al., 2015). Also, more metabolically stable cholinomimetic ligands can be obtained as heterocycles, such as 1,3,4-thiadiazole ring, can act as a bio-isostere to replace the ester group of the neurotransmitter ACh (Patani and LaVoie, 1996).

On the other hand, the bulky tricyclic hydrocarbon with a cage-like structure that is called adamantane has also many characteristic features besides its previously approved wide pharmacological activities as shown in Figure 3 (Spilovska et al., 2016; Stockdale and Williams, 2015). These features include enhancement for lipophilicity, pharmacokinetic parameters, BBB permeability (Wishnok, 1973), hydrophobic interactions and rigid spatial arrangement. Also, adamantane enhances the duration of action as its bulk nature provides protection from metabolic degradation for close functional groups (Lamoureux and Artavia, 2010; Wanka et al., 2013).

Considering all the above-mentioned findings, novel series of *N*-[5-(adamantan-1-yl)-1,3,4-thiadiazol-2-yl]-2-(4-un/substituted) cyclic secondary amino-acetamide **(3a–3j)**/propanamide **(4a–4g)** were synthesized and evaluated *in vitro* as MTD against AChE, BChE, *h*-MAO-A and *h*-MAO-B enzymes for AD. The purity and chemical structures were confirmed by utilizing infrared

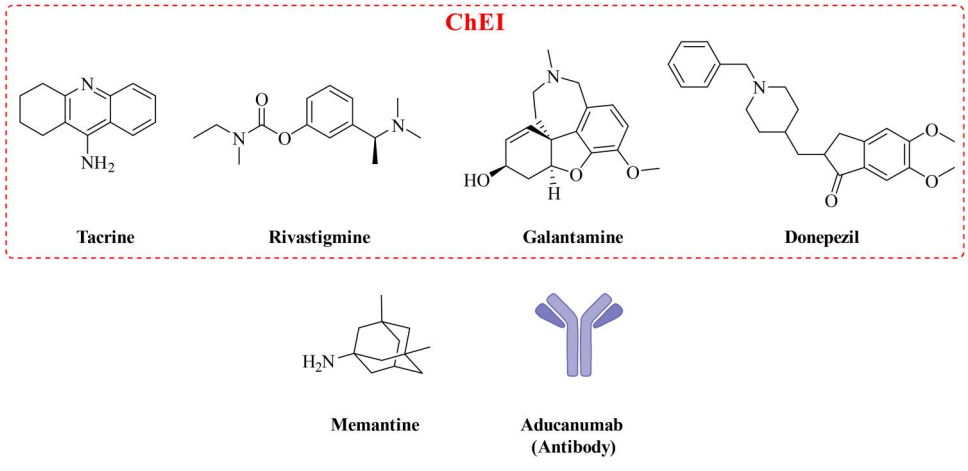

Figure 1. FDA-approved drugs for AD.

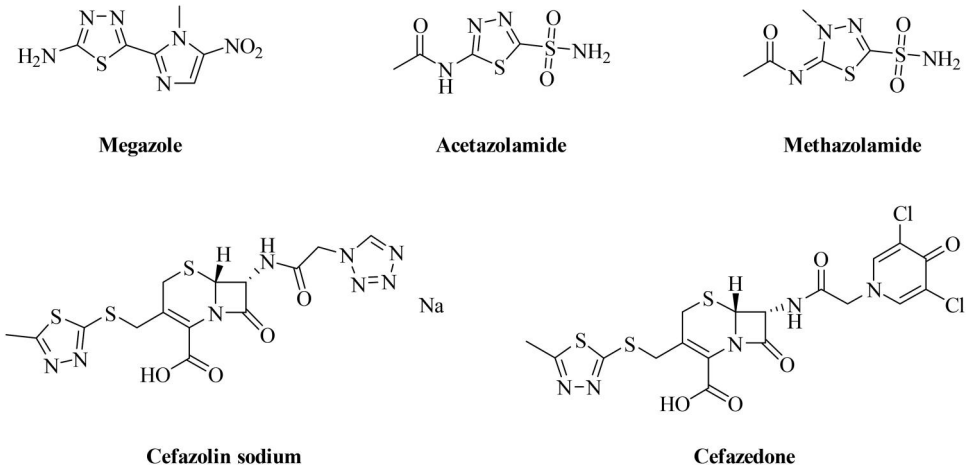

Figure 2. Drugs containing 1,3,4-thiadiazole ring.

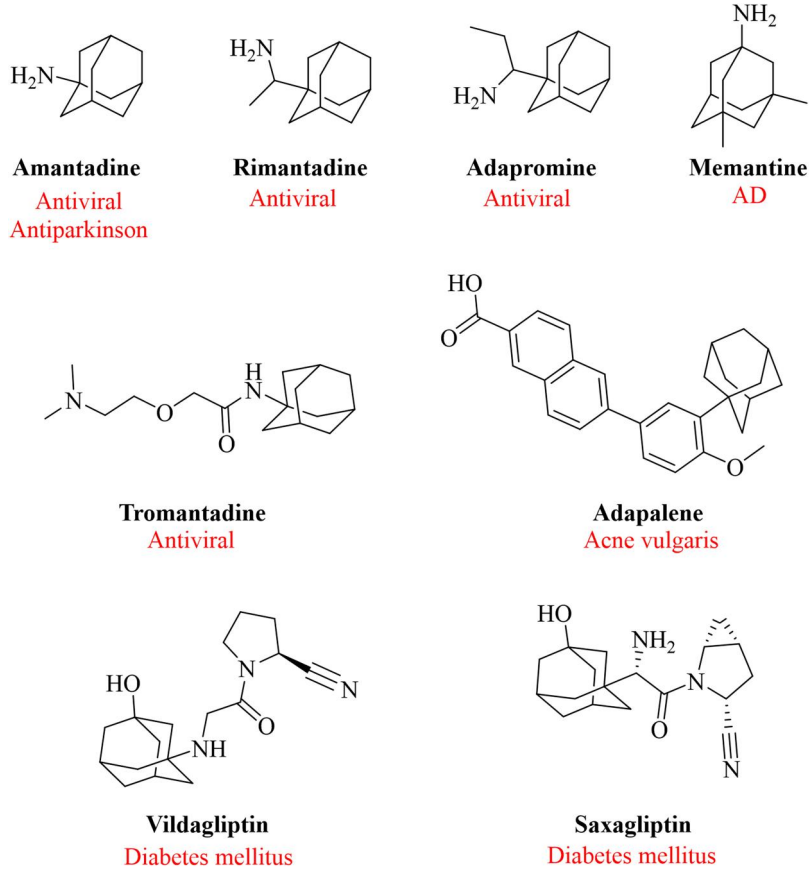

Figure 3. Drugs containing adamantane.

spectrometry (IR), proton nuclear magnetic resonance (^{1}H-NMR) spectrometry, carbon nuclear magnetic resonance (^{13}C-NMR) spectrometry and high-resolution mass spectrometry (HRMS), while molecular modeling studies including molecular docking and MDS were carried out to investigate the nature of binding for the most active derivatives.

Results and discussion

Chemistry

A total of seventeen *N*-[5-(adamantan-1-yl)-1,3,4-thiadiazol-2-yl]-2-(4-un/substituted) cyclic secondary amino-acetamide/propanamide derivatives were synthesized following two pathways, each with three steps synthetic procedures as shown in Scheme 1. The two pathways in the order of (A→B→D) and (A→C→E) for synthesizing the derivatives **(3a–3j)** and **(4a–4g)**, respectively share the first step (A) to cyclize 5-(adamantan-1-yl)-1,3,4-thiadiazol-2-amine **(1)** starting from 1-adamantane carboxylic acid by using $POCl_3$ as a dehydrating agent. On the other hand, the second step in both pathways (B vs. C) differs in terms of the nature of the acetylating agent as chloroacetyl chloride was used in B procedure and 2-chloropropionyl chloride was used in C procedure to synthesize *N*-[5-(adamantan-1-yl)-1,3,4-thiadiazol-2-yl]-2-chloroacetamide **(2a)** and *N*-[5-(adamantan-1-yl)-1,3,4-thiadiazol-2-yl]-2-chloropropanamide **(2b)**, respectively. The third step in

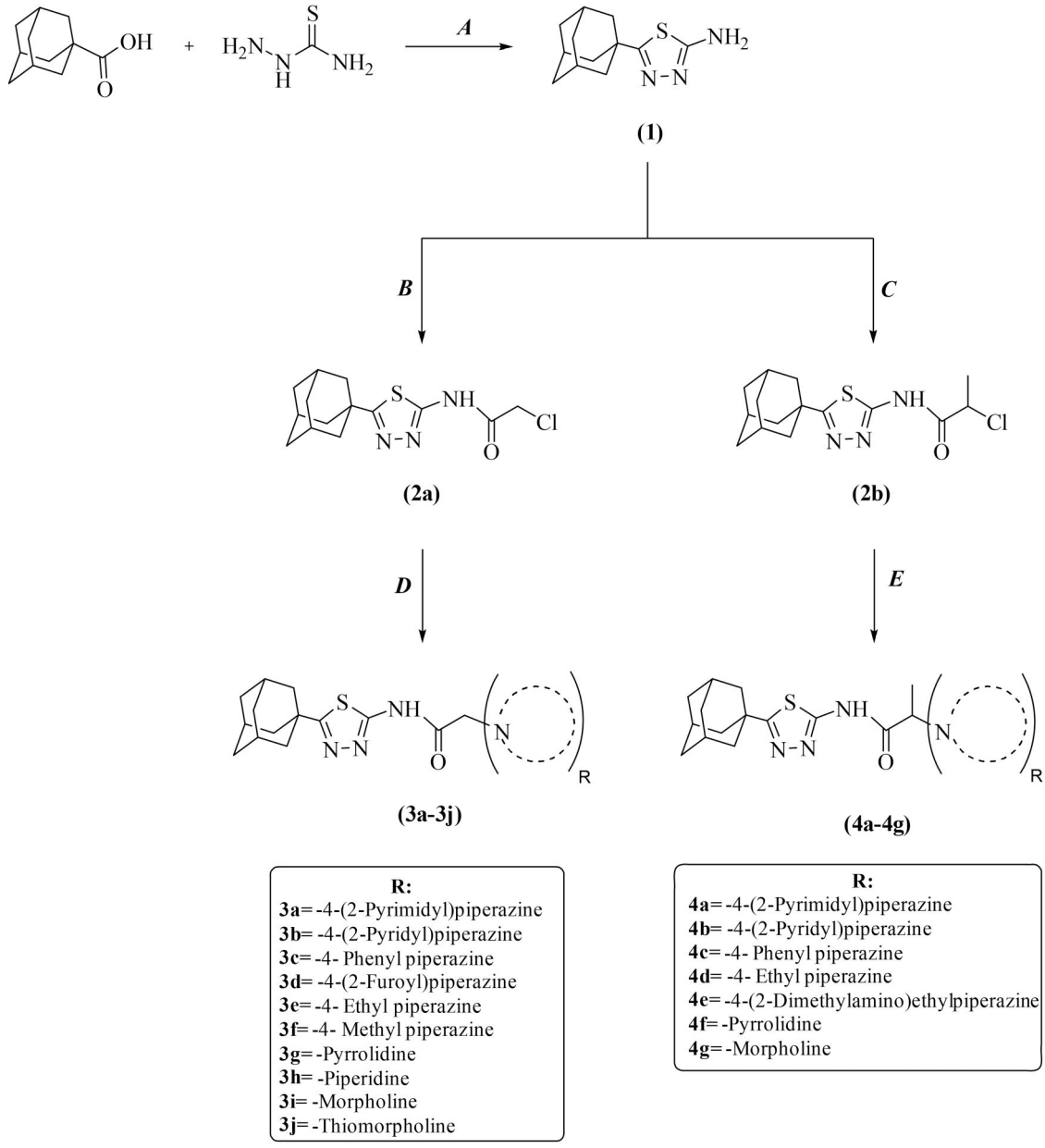

Scheme 1. General synthesis of the targeted compounds. (A) $POCl_3$, H_2O, Δ, 4–5 hrs; (B) $ClCH_2COCl$, THF, TEA, ice bath, 3-4hrs; (C) $ClCOCH(Cl)CH_3$, THF, TEA, ice bath, 3-4 hrs; (D) THF, TEA, R.T., 12-24 hrs; E: ACN, K_2CO_3, Δ, 12-24 hrs.

both pathways (D vs. E) differs in terms of the reaction conditions as different cyclic secondary amine derivatives were reacted separately with *N*-[5-(adamantan-1-yl)-1,3,4-thiadiazol-2-yl]-2-chloroacetamide **(2a)** in THF/TEA at room temperature and with *N*-[5-(adamantan-1-yl)-1,3,4-thiadiazol-2-yl]-2-chloropropanamide **(2b)** in ACN/K_2CO_3 at 80–100 °C as in procedures D and E, respectively. The conditions of the reaction which are THF/TEA solution at room temperature were planned to be the same for compounds **3a–3j** and **4a–4g,** however, the conditions were re-optimized for compounds **4a–4g** as the progression and yield were too low, and harsher conditions which are ACN/K_2CO_3 at reflux were applied. The reason that compounds **4a–4g** need harsher conditions can be attributed back to the presence of that extra methyl group which introduces both a tertiary methine carbon and a steric hindrance for the nucleophilic attack in this reaction.

All final synthesized compounds were recrystallized from ethanol and the yield was in the range of 55–96% for derivatives **3a–3j** while it was 50–74% for derivatives **4a–4g**. Purity and structure elucidation were confirmed by melting point analysis and spectral analysis using IR, ^{1}H-NMR, ^{13}C-NMR and HRMS. Spectral analysis results for the final targeted compounds are presented in Supplementary Figures S1–S68, while the spectral analyses of the intermediate compounds **1** and **2a** have previously been reported in the literature (Fesatidou et al., 2018; Wassel et al., 2021).

In IR spectra, the main common functional groups were observed as follows: N–H stretching of the amidic functional groups above 3000 cm^{-1}; sp^3 C–H stretching in the range of 2974–2777 cm^{-1}; C = O of the amidic functional group in the range of 1687–1734 cm^{-1}; aromatic C = C and C = N stretching at 1597–1290 cm^{-1} and C–N stretching at 1305–1014 cm^{-1}.

In ^{1}H NMR spectra, protons of the adamantane ring were seen in the range of chemical shifts of 1.68–2.10 ppm as three

signals for all derivatives except for **3e**, **4c** and **4f** which have two signals. For most derivatives, the amidic proton was noticed in the range of 10.53–12.64 ppm as a broad singlet peak. The protons of both the methylene group in compounds **3a–3j** and the methine group in compounds **4a–4g** were seen in the general range of 3.24–4.03 ppm while protons of the $-CH_3$ within the propanamide group in derivatives **4a–4g** have a doublet signal with a chemical shift of 1.14–1.40 ppm except in compound **4a** and compound **4e** which have a broad singlet peak in the same general range. The secondary cyclic amine substituents were seen as follows, piperazine's protons in the range of 2.22–3.75 ppm; pyrrolidine's protons in the range of 1.68–2.69 ppm; piperidine's protons in the range of 1.33–2.44 ppm; morpholine's protons in the range of 2.43–3.57 ppm and thiomorpholine's protons in the range of 2.6–2.73 ppm. Moieties attached to the fourth position of piperazine were noticed as following, pyrimidinyl's protons have two signals that are a triplet peak at 6.59–6.60 ppm and a doublet/broad singlet at 8.31–8.34 ppm; pyridinyl's protons have four signals that are a triplet signal at 6.59–6.62 ppm, a doublet signal at 6.77–6.80 ppm, a triplet signal at 7.48–7.51 ppm and a doublet signal at 8.07–8.09 ppm; phenyl's protons have three signals that are a triplet peaks at 6.67 and 6.86 ppm, a doublet peaks at 6.91 and 6.95 ppm and a triplet peaks at 7.19 and 7.29 ppm in derivatives **3c** and **4c**, respectively; furoyl's protons in derivative **3d** have three signals that are a triplet signal at 6.6 ppm, a doublet signal at 6.97 ppm and a singlet signal at 7.82 ppm; the aliphatic ethyl's protons have two signals that are a triplet peaks of the $-CH_3$ at 0.94 and 1.10 ppm and a signal of the $-CH_2-$ at 2.22 and 2.46 ppm in derivatives **3e** and **4d**, respectively; the aliphatic methyl's protons in derivative **3f** have a singlet signal at 2.14 ppm; and the aliphatic *N, N*-dimethylaminoethyl moiety in derivative **4e** have a singlet signal of the two methyl groups at 2.12 ppm and a signal of the aminoethyl's protons in the range of 2.95–3.47 ppm.

In ^{13}C NMR spectra, carbons of the adamantane ring were noticed upfield to the right of the spectra in the range of 28.29–43.57 ppm as four signals, while 1,3,4-thiadiazole ring's carbons were seen downfield to the left of the spectra in the range of 157.21–172.86 as two signals. The most deshielded signal in the range of 173.94–175.98 ppm was assigned to the amidic carbonyl carbon. The carbon of the methylene group in compounds **3a–3j** and methine group in compounds **4a–4g** has a signal in the general range of 57.94–61.61 ppm and 62.09–66.85 ppm, respectively while the carbon of the $-CH_3$ within the propanamide group in derivatives **4a–4g** has a signal in the range of 10.97–15.40 ppm. Carbons of the secondary cyclic amine substituents were found to have signals in the general range of 23.47–66.55 ppm while aromatic substituents attached to the fourth position of piperazine were seen in the range of 107.42–163.48 ppm and aliphatic ones in the range of 11.96–56.94 ppm. For derivative **3d**, a signal of the carbonyl group that links piperazine and furan rings was seen at 158.7 ppm.

In HRMS spectra, no impurities were noticed in the chromatograms and $[M+1]$ peaks of all final derivatives are consistent with their expected molecular weights.

Table 1. Pharmacokinetic parameters of the active compounds **3a**, **3b**, **3d**, **4a** and **4b**.

Cpd.	MW[a]	HBA[a]	HBD[a]	MLogP[a]	LogS[a]	BBB score[b]	GIA[a]	DLS[b]	No.V[a]
3a	439.58	6	1	1.88	−4.35	3.82	High	1.49	0
3b	438.59	5	1	2.48	−4.75	4.21	High	1.35	0
3d	455.57	6	1	1.65	−4.42	3.36	High	1.30	0
4a	453.6	6	1	2.09	−4.68	3.79	High	1.71	0
4b	452.62	5	1	2.69	−5.08	4.17	High	1.46	0
Donepezil	379.49	4	0	3.06	−4.81	5.29	High	1.56	0
Selegiline	187.28	1	0	3.25	−2.88	4.89	High	0.85	0

Cpd.: compound, MW: molecular weight (g/mol), HBA: number of hydrogen bond acceptors, HBD: number of hydrogen bond donors, MLog P: octanol/water partition coefficient, Log S: aqueous solubility (highly soluble > 0 > very soluble > −2 > soluble > −4 > moderately soluble > −6 > poorly soluble > −10 > insoluble), BBB score: blood–brain barrier score ranges from the lowest 0 to the highest six penetration, GIA: gastrointestinal absorption, DLS: drug-likeness score (0–2) and No.V: number of Lipinski's rule Violation. [a]Calculated using SwissADME software. [b]Calculated using Molsoft software.

ADME parameters

By using*in silico* SwissADME (Daina et al., 2017, 31) and Molsoft (32) web tools, an early prediction of ADME parameters (absorption, distribution, metabolism and elimination) was obtained for the most active derivatives and standard drugs as illustrated in Table 1. Based on the obtained physicochemical results, the synthesized derivatives were found to have a favorable pharmacokinetic profile that is in line with their pharmacological activity which boosts the drug-likeness of these derivatives as they have no more than one violation of Lipinski's rule with molecular weights less than 500, hydrogen bond donor = 1, hydrogen bond acceptors = 5-6 and octanol/water partition coefficient (MLogP) varied from 1.65 to 2.69. Besides that, aqueous solubility (Log S), gastrointestinal membrane permeability (GIA) and more importantly BBB permeability values were also within acceptable ranges.

In-vitro cholinesterase and MAO inhibition activity studies

The percent of inhibition (% inhibition) of the synthesized compounds against AChE, BChE, *h*-MAO-A and *h*-MAO-B were first evaluated at concentrations of 10^{-3} M and 10^{-4} M as shown in Table 2. Derivatives **4a**, **4b**, **3a**, **3d** and **3b** which showed more than 50% inhibition were further investigated at lower concentrations (10^{-5}–10^{-9} M) to calculate their IC_{50} concentrations as shown in Table 3 and Supplementary Figures S69 and S70.

The synthesized compounds were more selective and potent toward AChE compared to BChE with derivatives **4a**, **4b**, **3a**, **3d** and **3b** expressing high AChE inhibition activity from the most active to the least ones. Among these compounds, compound **4a** which carries a pyrimidinyl moiety at the fourth position of the piperazine ring showed the most inhibition activity against AChE with an IC_{50} value that is the closest to that of donepezil (0.036 vs. 0.0201 μM). Replacing pyrimidinyl moiety with pyridinyl in compound **4b** results in an IC_{50} value of 0.052 μM, while the absence of the methyl group in the structure of compound **3a** leads to an inhibition activity that is 1.8 times lower than that of compound **4a** with an IC_{50} value of 0.067 μM. Compared to **3a**, compound **3d** which carries furoyl moiety instead of pyrimidinyl has an IC_{50} of 0.159 μM, while compound **3b** which carries

Table 2. Initial screening and % inhibition at 10^{-3} and 10^{-4} M concentrations of the synthesized compounds, donepezil, tacrine, moclobemide and selegiline against AChE, BChE, h-MAO-a and h-MAO-B.

	AChE% inhibition		BChE% inhibition		MAO-A% inhibition		MAO-B% inhibition	
Compounds	10^{-3} M	10^{-4} M	10^{-3} M	10^{-4} M	10^{-3} M	10^{-4} M	10^{-3} M	10^{-4} M
3a	**92.152 ± 2.422**	**87.676 ± 1.703**	31.521 ± 0.832	27.608 ± 0.751	39.166 ± 1.321	31.059 ± 0.959	**85.667 ± 1.927**	**82.385 ± 2.144**
3b	**86.759 ± 1.069**	**81.334 ± 0.964**	28.236 ± 0.958	22.132 ± 0.809	37.648 ± 0.966	26.684 ± 0.832	**72.142 ± 2.052**	42.366 ± 0.892
3c	**67.647 ± 1.833**	39.086 ± 0.897	32.320 ± 1.063	24.761 ± 0.822	41.377 ± 1.395	34.651 ± 1.197	41.585 ± 1.068	36.274 ± 0.857
3d	**90.182 ± 1.933**	**84.567 ± 2.254**	27.608 ± 0.847	21.459 ± 0.885	36.289 ± 0.922	27.469 ± 0.874	46.752 ± 0.866	28.651 ± 0.721
3e	**79.432 ± 2.197**	41.362 ± 0.922	36.747 ± 1.055	23.841 ± 0.947	40.760 ± 1.558	30.324 ± 1.047	**68.823 ± 1.833**	40.536 ± 1.090
3f	**82.595 ± 1.958**	48.814 ± 1.257	31.089 ± 1.157	20.262 ± 0.844	42.417 ± 1.751	28.131 ± 0.875	44.654 ± 0.928	39.614 ± 0.957
3g	49.346 ± 0.957	40.134 ± 0.951	29.834 ± 0.974	23.075 ± 0.775	43.668 ± 1.907	30.866 ± 0.920	48.890 ± 0.974	40.159 ± 0.962
3h	43.487 ± 1.084	34.424 ± 0.729	34.959 ± 1.162	26.966 ± 0.875	37.923 ± 1.155	32.526 ± 0.963	45.961 ± 0.811	37.421 ± 0.833
3i	48.090 ± 0.862	36.797 ± 0.874	38.267 ± 1.285	23.620 ± 0.896	34.439 ± 0.947	27.941 ± 0.885	**62.422 ± 1.658**	42.744 ± 1.108
3j	**53.741 ± 0.731**	42.551 ± 0.933	30.059 ± 0.957	20.448 ± 0.964	38.121 ± 1.223	25.134 ± 0.874	**68.241 ± 1.921**	46.864 ± 0.857
4a	**94.239 ± 2.356**	**92.787 ± 2.150**	27.111 ± 0.850	22.195 ± 0.917	40.048 ± 1.675	33.259 ± 1.097	**93.471 ± 2.436**	**89.286 ± 1.923**
4b	**92.848 ± 1.957**	**89.561 ± 1.824**	28.457 ± 1.011	21.011 ± 0.823	42.555 ± 1.035	38.047 ± 0.929	**91.552 ± 1.866**	**88.679 ± 2.144**
4c	46.637 ± 1.041	35.364 ± 0.889	32.962 ± 1.389	27.336 ± 0.970	39.699 ± 0.984	31.697 ± 0.752	**56.109 ± 1.174**	41.666 ± 0.721
4d	**79.723 ± 2.374**	48.215 ± 1.002	24.663 ± 0.959	20.547 ± 0.830	46.862 ± 1.427	32.586 ± 0.961	**74.663 ± 1.336**	40.528 ± 0.968
4e	48.190 ± 1.421	40.658 ± 1.097	32.549 ± 1.089	20.652 ± 0.851	40.723 ± 1.021	36.838 ± 0.964	48.358 ± 0.855	36.423 ± 0.959
4f	**81.525 ± 1.727**	39.438 ± 0.944	34.174 ± 0.867	24.112 ± 0.958	47.318 ± 0.839	32.122 ± 0.874	**52.754 ± 1.328**	32.241 ± 0.836
4g	42.827 ± 0.879	38.790 ± 0.985	33.464 ± 0.966	28.247 ± 0.958	46.864 ± 1.636	32.657 ± 1.057	**77.921 ± 1.878**	39.070 ± 0.836
Donepezil	99.156 ± 1.302	97.395 ± 1.255	–	–	–	–	–	–
Tacrine	–	–	99.827 ± 1.378	98.675 ± 1.450	–	–	–	–
Moclobemide	–	–	–	–	94.121 ± 2.760	82.143 ± 2.691	–	–
Selegiline	–	–	–	–	–	–	98.589 ± 2.055	94.850 ± 1.114

Table 3. IC_{50} (μM) against AChE and h-MAsO-B based on the % inhibition from 10^{-3} to 10^{-9} M concentrations of compounds **3a**, **3b**, **3d**, **4a** and **4b**, donepezil and selegiline.

Compounds	AchE IC_{50} (μM)	MAO-B IC_{50} (μM)
3a	0.067 ± 0.003	0.402 ± 0.018
3b	0.288 ± 0.011	–
3d	0.159 ± 0.006	–
4a	**0.036 ± 0.001**	0.054 ± 0.002
4b	0.052 ± 0.002	0.141 ± 0.006
Donepezil	0.0201 ± 0.0010	–
Selegiline	–	0.0374 ± 0.0016

pyridinyl moiety instead of pyrimidinyl has an IC_{50} of 0.288 μM.

Consistent with the results of the anticholinesterase activity of these derivatives, it was found that **4a**, **4b** and **3a** were also the active ones against *h*-MAO-B, making them dual inhibitor drug candidates, while no significant activity was recorded against *h*-MAO-A for all derivatives. Among these derivatives, compound **4a** is the most active one against *h*-MAO-B with an IC_{50} of 0.054 μM compared to that of the standard drug selegiline (IC_{50} = 0.0374 μM), while the other two derivatives **4b** and **3a** show moderate inhibition activity with IC_{50} of 0.141 and 0.402 μM, respectively.

Based on the structure-activity relationship (SAR), it is concluded that (Figure 4):

- The potency of active compounds was increased when R_1 is a methyl group compared to H.
- Derivatives that contain piperazine ring (R_2 = N) were more active than those with other cyclic secondary amines (R_2 = S, O, C).
- The presence of heterocyclic aromatic substituents at the fourth position of the piperazine ring (R_3) has a positive effect on the activity, the pyrimidinyl scaffold showed the best effects.
- The size of the secondary cyclic amine ring has not a prominent effect on the inhibition activity (pyrrolidine vs. piperidine).

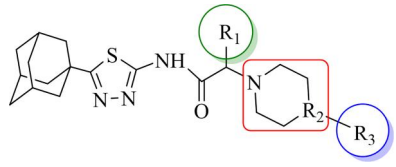

Figure 4. Structure-activity relationship of the synthesized derivatives.

Molecular docking studies

The binding interactions of the most active derivatives within the active sites of the related enzymes were investigated using molecular docking and molecular dynamic simulation (MDS) studies to examine the crucial bonds, the nature and the stability of the binding that are essential for active molecules.

Docking study on AChE enzyme

Derivatives **4a**, **4b** and **3a** which displayed the highest inhibition activity against AChE were investigated within the enzyme's active site. As shown in the 2D poses (Figures 5–7) and the 3D poses (Figures 8–10), all three derivatives can be considered as dual binding site inhibitors as they bind to both the central catalytic anionic site (CAS) and the peripheral anionic site (PAS) with a total of seven binding interactions (Table 4). Two common binding interactions were formed at PAS by all derivatives **4a**, **4b** and **3a** which are a π–π stacking interaction of Trp286 residue with the 1,3,4-thiadiazole ring and a π-cation interaction of Tyr341 residue with the positive ionized piperazine's nitrogen. These interactions were reported as crucial ones for many potent AChEI (Cheung et al., 2012). Also, ligands that were able to form binding interactions within PAS are considered to have a secondary non-cholinergic effect associated with their ability to decrease the formation of the neurotoxic Aβ aggregates in AD by blocking the access of the fibrils of Aβ peptides to this peripheral site to form stable AChE-Aβ complexes

Table 4. Interaction index for the active compounds-AChE complex.

Compounds	Ligand moiety	Binding site, residue	Interaction type, count	Bond distance (Å)
3a	1,3,4-thiadiazole ring	PAS, Trp286	π–π stacking, 1	5.33
	Positive ionized piperazine's nitrogen	PAS, Tyr341	π-cation, 1	4.30
	N_3 of the 1,3,4-thiadiazole ring	CAS, Phe295	H-bond, 1	2.17
	Positive ionized piperazine's nitrogen	CAS, Tyr337	π-cation, 1	5.33
	Hydrogen at C_4 of pyrimidine	CAS, Glh202	Ar H-bond, 1	2.79
	Hydrogen at C_3 Pyrimidine ring	CAS, His447	Ar H-bond, 1	2.67
	Pyrimidine ring	CAS, His447	π–π stacking, 1	4.94
4a	1,3,4-thiadiazole ring	PAS, Trp286	π–π stacking, 1	5.31
	Positive ionized piperazine's nitrogen	PAS, Tyr341	π-cation, 1	4.93
	N_3 of the 1,3,4-thiadiazole ring	CAS, Phe295	H-bond, 1	2.95
	Positive ionized piperazine's nitrogen	CAS, Tyr337	π-cation, 1	5.32
	Hydrogen at C_5 of pyrimidine	CAS, Glh202	Ar H-bond, 1	2.61
	Hydrogen at C_4 of pyrimidine	CAS, His447	Ar H-bond, 1	2.70
	Positive ionized piperazine's nitrogen	CAS, Trp86	π-cation, 1	5.64
4b	1,3,4-thiadiazole ring	PAS, Trp286	π–π stacking, 1	5.45
	Positive ionized piperazine's nitrogen	PAS, Tyr341	π-cation, 1	4.68
	N_3 of the 1,3,4-thiadiazole ring	CAS, Phe295	H-bond, 1	2.17
	Positive ionized piperazine's nitrogen	CAS, Tyr337	π-cation, 1	5.13
	Hydrogen at C_4 of the pyridine	CAS, Glh202	Ar H-bond, 1	2.51
	Pyridine	CAS, Trp86	π–π stacking, 1	4.42
	Positive ionized piperazine's nitrogen	CAS, Trp86	π-cation, 1	4.23

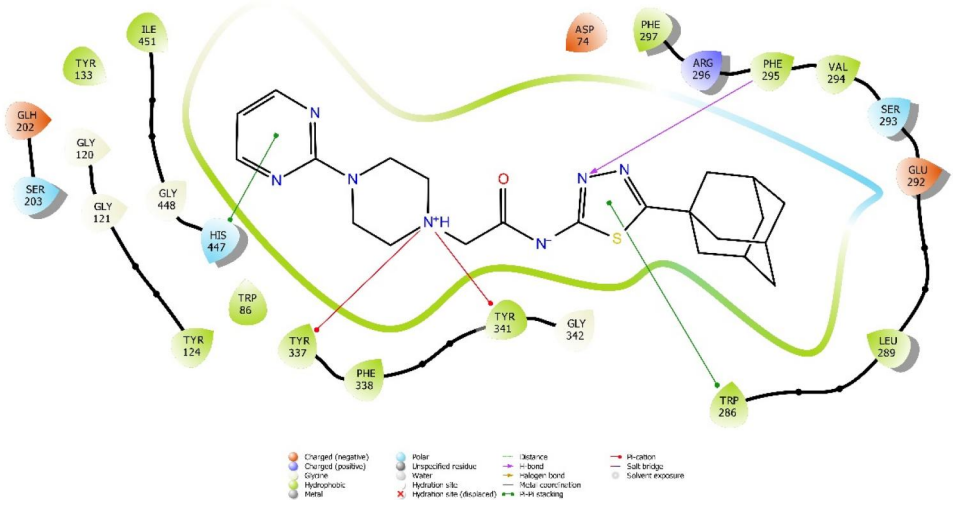

Figure 5. 2D Poses of the interaction of AChE with compound **3a**.

(Alvarez et al., 1997). Other three common binding interactions in all three derivatives were noticed within the CAS which are a hydrogen bond interaction of Phe295 with N_3 of the 1,3,4-thiadiazole ring, a π-cation interaction of Tyr337 with the positive charged piperazine's nitrogen and an aromatic hydrogen bond interaction (Ar H-bond) between the carbonyl oxygen of Glh202 and the hydrogen at C_4 of the pyridine (**4b**) or the hydrogen at C_5 of pyrimidine (**4a** and **3a**).

Besides that, the third most active compound **3a** forms two additional binding interactions between His447 and the pyrimidine ring, the first is a π–π stacking interaction and the second is an Ar H-bond interaction. The second most active compound **4b** forms two additional binding interactions with the crucial amino acid Trp86, the first is a stacking π–π interaction with pyridine and the second is a π-cation interaction with the positively charged piperazine's nitrogen. However, the first most active compound **4a** was found to maintain a balanced pattern of binding interactions with both His447 and Trp86 residues. The former residue's carbonyl oxygen forms an Ar H-bond interaction with the hydrogen at C_4 of the pyrimidine. In contrast, the latter residue's indole ring forms a π-cation interaction with the piperazine's positively charged nitrogen. As noticed, the absence of the interaction with Trp86 causes a more significant decrement in the activity of compound **3a** than the absence of the interaction with His447 as in compound **4b**.

Docking study on h-MAO-B enzyme

Binding interactions of derivative **4a** that displayed the most inhibition activity against *h*MAO-B were studied and presented in Figure 11 as 2D and 3D poses. Generally, the derivative **4a** was well located near the Flavin adenine dinucleotide (FAD) coenzyme. It participates in seven binding interactions (Table 5), four of which involve the pyrimidine ring. The most important one among these four bonds is the one that involves Tyr435 residue in a π–π stacking interaction as it also presents in many other potent compounds

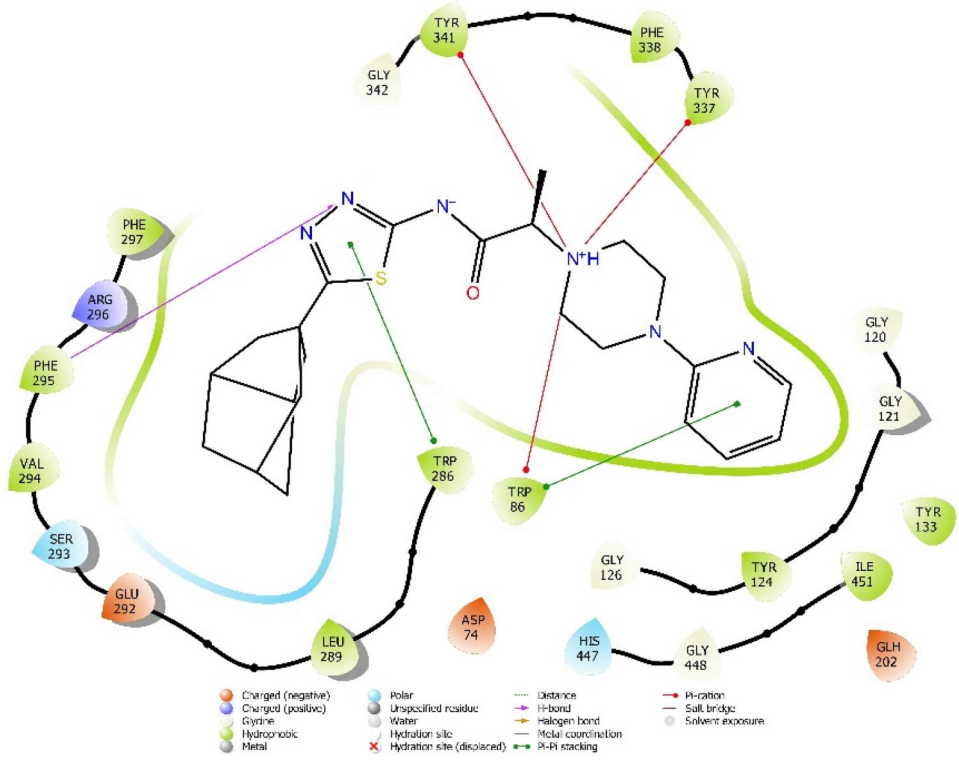

Figure 6. 2D Poses of the interaction of AChE with compound **4b**.

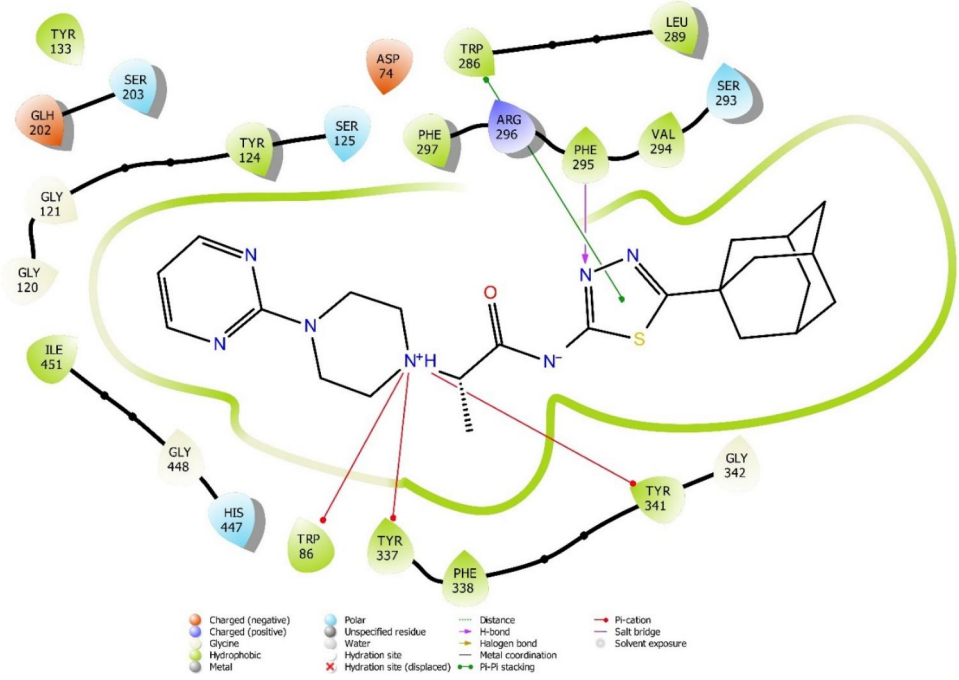

Figure 7. 2D Poses of the interaction of AChE with compound **4a**.

interactions (Can et al., 2017). The other three are all Ar H-bond interactions, two with Tyr434 and the last with Cys172 residue. The amino acid residue Tyr326 was involved in two binding interactions, the first is another π–π stacking interaction with the 1,3,4-thiadiazole ring and the second is an Ar H-bond interaction with the amidic carbonyl oxygen. The amino acid residue Gln 206 which was found to affect the selectivity for MAO-B (Evren et al., 2022) participates in an H-bond interaction with the piperazine's ionized positive nitrogen atom.

Molecular dynamic simulation (MDS) studies

Derivative **4a** which showed dual inhibition activity against AChE and *h*MAO-B was studied further through MDS to investigate the nature of binding interactions. The radius of

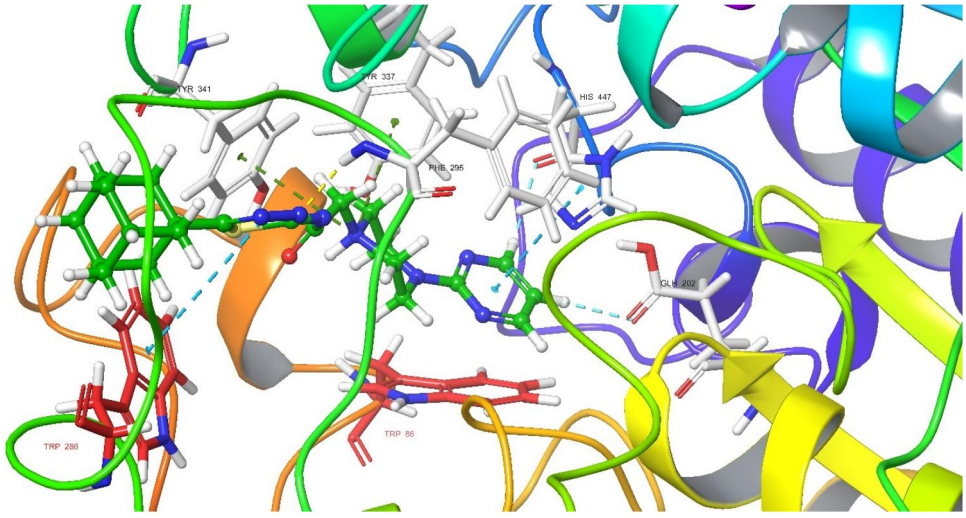

Figure 8. 3D Pose of the interaction of compound **3a** with AChE.

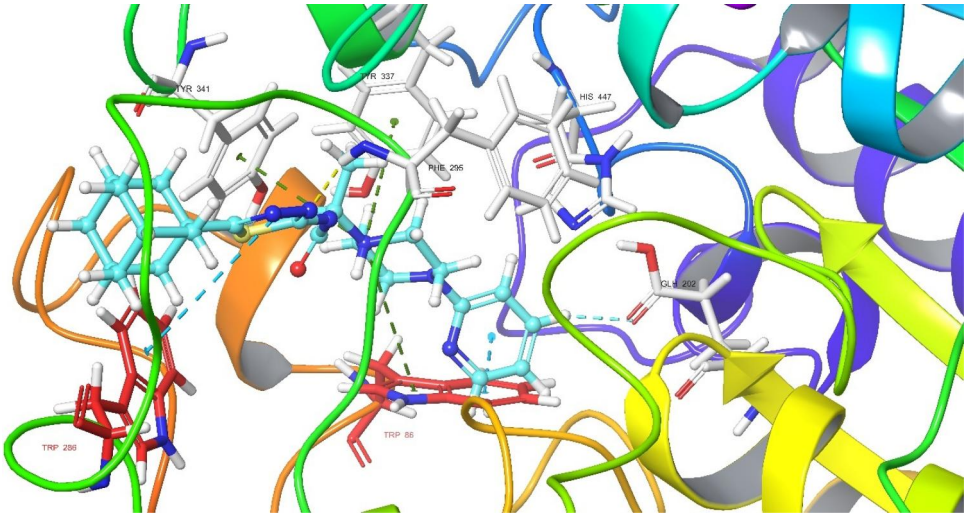

Figure 9. 3D Pose of the interaction of compound **4b** with AChE.

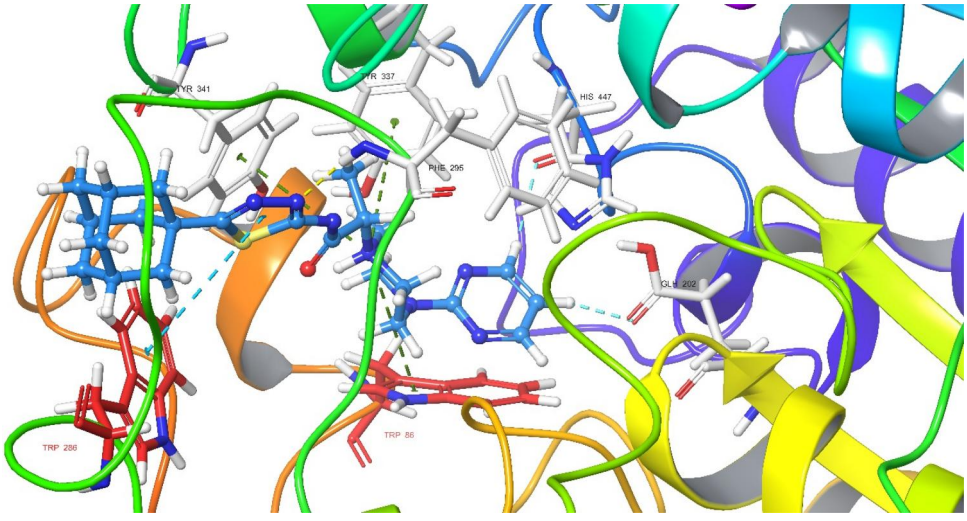

Figure 10. 3D Pose of the interaction of compound **4a** with AChE.

Table 5. Interaction index for the active compounds-MAO-B complex.

Compound	Ligand moiety	Residue	Interaction type, count	Bond distance (Å)
4a	Pyrimidine ring	Tyr435	π–π stacking, 1	3.57
	Pyrimidine ring	Tyr434	Ar H-bond, 2	2.56, 2.48
	Pyrimidine ring	Cys172	Ar H-bond, 1	2.44
	1,3,4-thiadiazole ring	Tyr326	π–π stacking, 1	5.05
	Amidic carbonyl oxygen	Tyr326	Ar H-bond, 1	2.49
	Positive ionized piperazine's nitrogen	Gln 206	H-bond, 1	1.83

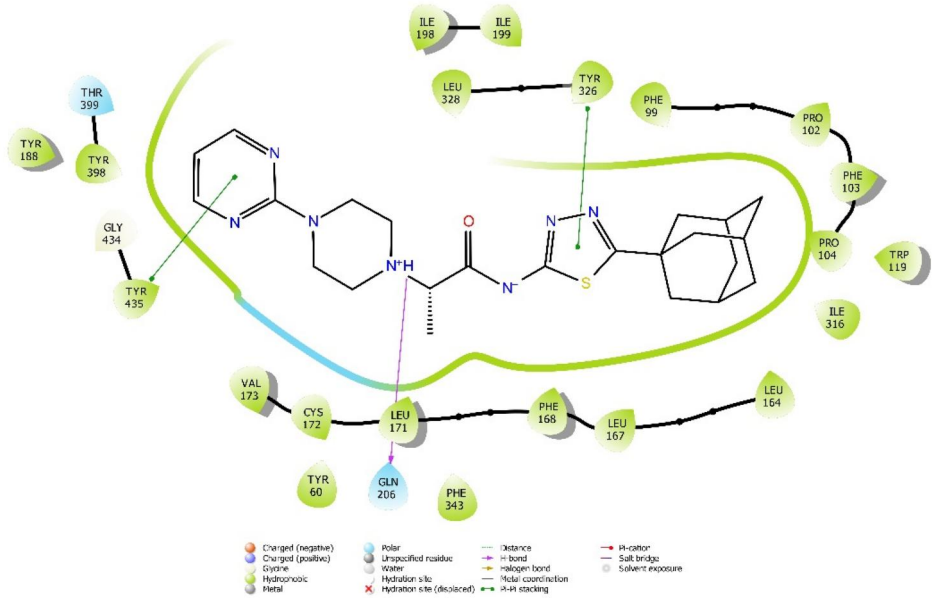

(a)

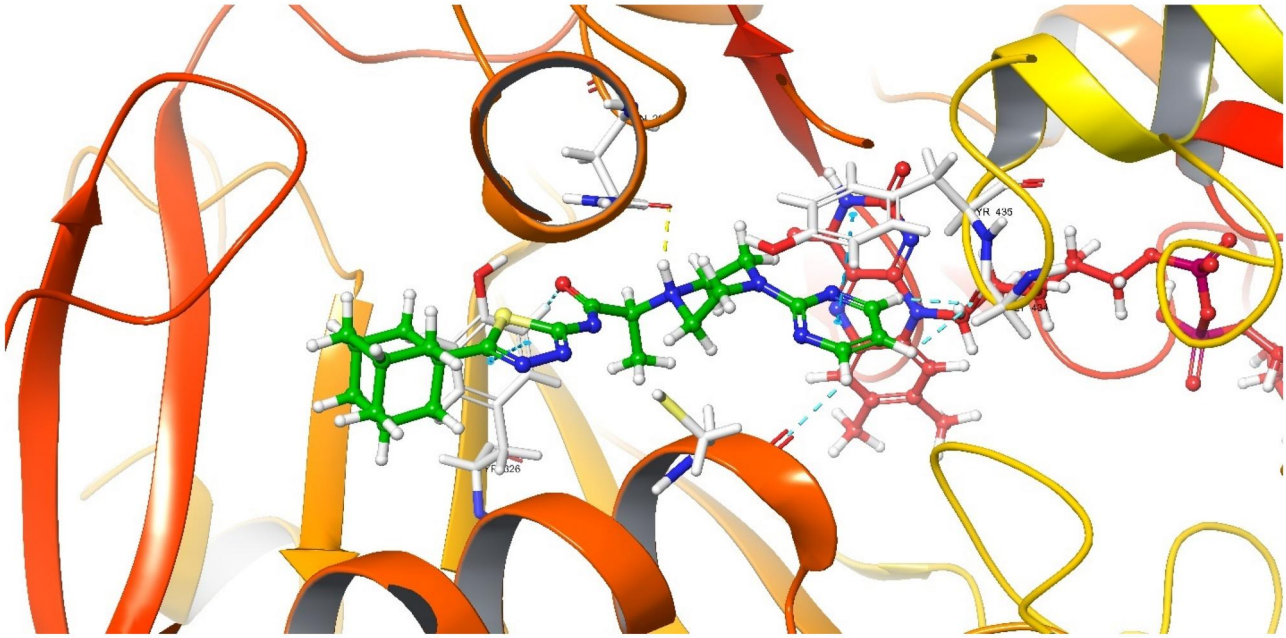

(b)

Figure 11. The interaction of compound **4a** with hMAO-B; 2D pose (a) and 3D pose (b).

gyration (R_g), root-mean-square fluctuation (RMSF) and root square deviations (RMSD) values were calculated to indicate the stability of the derivative-enzyme complex.

MDS on 4a and AChE complex

Data obtained from MDS of derivative **4a** within AChE were represented in Supplementary Figure-S71 and Figure12. As

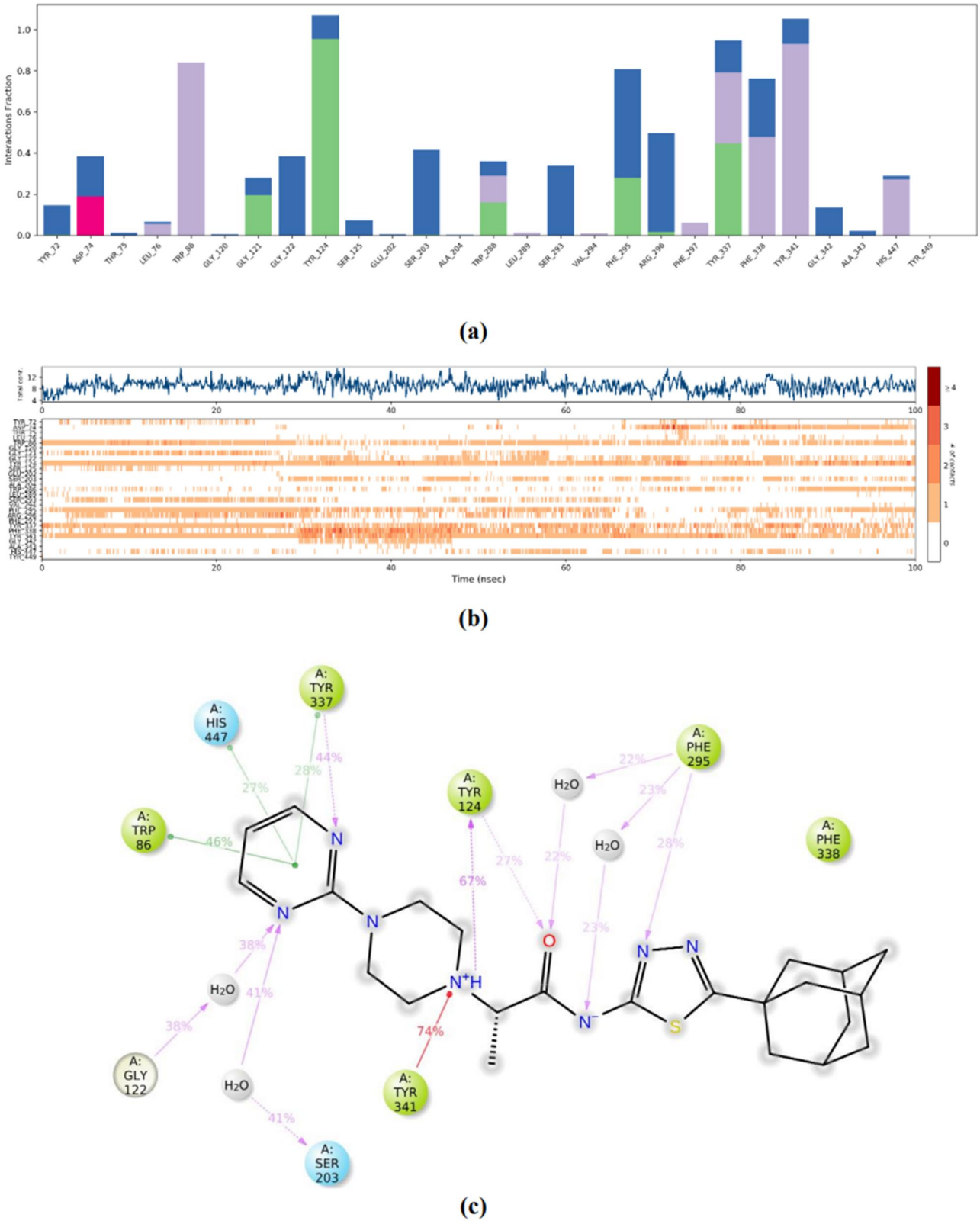

Figure 12. MDS studies of ligand **4a** within AChE. The plots of (a) the interactions fraction-residue, (b) the residue-time and (c) the diagram of contact strength (cutoff = 30%) as 2D pose.

shown in Figure S71, the complex shows high stability throughout the simulation, as the R_g plot is consistent with minimal fluctuations. Also, the RMSD value of the protein is within the acceptable range of 1–3 Å during the entire simulation which indicates the minimal conformation changes and stability of the protein. As expected, the rigid protein structures α-helices (red areas) and β-strands (blue areas) have minimal fluctuations compared to loop regions (white areas), thus RMSF value is an additional proof of the complex stability.

Binding interactions were presented in different ways as shown in Figure 12 and Supplementary Video 1. Generally, these interactions are noticed to be mainly and constantly with

Tyr124, Tyr341, Tyr337, Phe295, Phe338 and Trp86 residues. The π–π stacking interactions were observed to involve the pyrimidine moiety of derivative **4a** with Trp86, Tyr337 and His447. A π-cation interaction of the positively charged piperazine's nitrogen was formed with Tyr341. The H-bond interactions were formed with Tyr337, Tyr124 and Phe295, while the water-mediated H-bonds were formed with Gly122, Ser203 and Phe295. Besides that, Ar H-bonds were formed between the pyrimidine moiety of **4a** and the residues of Glh202, His404, Tyr337 and Gly121 (Supplementary Video 2) as well as between the amidic carbonyl oxygen and Phe297, Phe295, Tyr124 and Tyr341. The result of MDS is consistent with those in docking studies. As mentioned in the docking results section, inhibition of the AChE enzyme is significantly related to interacting with Trp86 (CAS region), thus, the interaction with this residue is the main explanation of the SAR. Another significant residue is Glh202, and the interaction with this amino acid may be connected to AChE selectivity, explaining why no inhibitory activity on BChE has been observed (Sağlık et al., 2016).

MDS on 4a and hMAO-B complex

As shown in Supplementary Figure S72, the complex has significant stability throughout the simulation. The R_g plot shows consistency with minimal fluctuations. The RMSD of protein indicates conformational stability as its value is within the acceptable range of 1–3 Å during the entire simulation. The RMSF value ensured the complex stability as α-helices (red areas) and β-strands (blue areas) have lower fluctuations than loop regions (white areas), however, no significant big fluctuations were observed between them.

As shown in Figure 13 and Supplementary Video 3, binding interactions with Tyr60, Phe343, Ser200, Thr201 and Gln206 were the dominant ones among others. A π-cation interaction was formed between the positively charged piperazine's nitrogen and Tyr60 residue. Both H-bond interactions and water-mediated H-bonds were seen with Ser200 and Thr201 residues. Water-mediated H-bonds were also noticed with Gln206 residue. Besides that, Ar H-bond interactions (Supplementary Video 4) were formed between pyrimidine's hydrogens of **4a** and Leu171, Cys172, Tyr398 and FAD protein as well as the amidic carbonyl oxygen of **4a** and both Tyr326 and Phe343 residues. The interactions with the FAD protein which acts as an H-bond acceptor enlighten the importance of incorporating polar groups that can act as H-bond donors at that position of the structure. In accordance with the previously mentioned docking results, interactions with Ser200, Thr201 and Gln206 residues were marked to be responsible for enzyme inhibition activity. Since propionamide moiety has a remarkable place in the interactions with those amino acids, this moiety can be a useful linker to design new MAO inhibitors (Çavuşoğlu et al., 2018; Kaya et al., 2016; Shen et al., 2014).

Materials and methods

Chemistry

All chemical substances were purchased from Acros Organics Chemicals (Acros Organics, USA), Fluka Chemicals (Germany), Sigma-Aldrich Chemical Co (Sigma-Aldrich Corp., St. Louis, MO, USA) and Merck Chemicals (Merck KGaA, Darmstadt, Germany). The Mettler Toledo-MP90 Melting Point System (Mettler Toledo, Ohio, USA) was used to measure melting point (m.p.) values of all final synthesized compounds that were uncorrected. Thin-layer chromatography (TLC) technique was used to monitor the progression of all reaction media using Silica Gel 60 F_{254} aluminum-covered plates (Merck KGaA, Darmstadt, Germany) as the stationary phase, while ethanol, 1:1 and 3:1 petroleum ether-ethyl acetate mixtures were used as the mobile phase. Chemical spectral analyses were recorded using the following instruments: Shimadzu-IR Affinity-IS instrument (Shimadzu, Japan); Bruker 300 MHz and 400 MHz NMR spectrometers (Bruker Bioscience, Billerica, MA, USA) in either DMSO-d_6 or $CDCl_3$ using TMS as internal standard; Shimadzu 8040 LC/MS/MS system (Shimadzu, Tokyo, Japan) was used to determine $M+1$ peaks. Analysis data including IR, ^{1}H-NMR, ^{13}C-NMR and HRMS of all final synthesized derivatives are provided to supplement data.

General synthesis of f 5-(adamantan-1-yl)-1,3,4-thiadiazol-2-amine (1)

An equal amount of 1-adamantane carboxylic acid (61.03 mmol, 11 g) and thiosemicarbazide (61.03 mmol, 5.56 g) were refluxed in phosphoryl chloride $POCl_3$ (40 ml) at 75–80 °C for half an hour. The reaction mixture was then cooled in an ice bath, cold distilled water (31 ml) was added dropwise and left for 15 mins. Again, the reaction mixture was refluxed for an additional 4–5 hrs. After the reaction was completed, it was cooled and neutralized in cold water with 2 N NaOH. The precipitated product was filtered and recrystallized from ethanol (Yang et al., 2012).

General synthesis of N-[5-(adamantan-1-yl)-1,3,4-thiadiazol-2-yl]-2-chloroacetamide (2a)

A stirred solution of 5-(adamantan-1-yl)-1,3,4-thiadiazol-2-amine **(1)** (25.49 mmol, 6 g) and TEA as a basic catalyst (30.6 mmol, 4.3 ml) in THF was first prepared. After that, a solution of chloroacetyl chloride in THF (30.6 mmol, 2.4 ml) was added dropwise to the stirred solution for 3-4 hrs at 0–5 °C. After the reaction was completed, THF was first evaporated and the residue was washed with water. The product was filtered and recrystallized from ethanol.

General synthesis of N-[5-(adamantan-1-yl)-1,3,4-thiadiazol-2-yl]-2-chloropropanamide (2b)

A stirred solution of 5-(adamantan-1-yl)-1,3,4-thiadiazol-2-amine **(1)** (25.49 mmol, 6 g) and TEA as a basic catalyst (30.6 mmol, 4.3 ml) in THF was first prepared. After that, a solution of 2-chloropropionyl chloride (30.6 mmol, 2.9 ml) in THF (30.6 mmol, 2.4 ml) was added dropwise to the stirred solution for 3–4 hrs at 0–5 °C. After the reaction was completed, THF was first evaporated, and the residue was washed with water. The product was filtered and recrystallized from ethanol.

General synthesis of N-[5-(adamantan-1-yl)-1,3,4-thiadiazol-2-yl]-2-substituted-acetamide derivatives (3a–3j)

At room temperature, an appropriate cyclic secondary amine (1.28 mmol) and *N*-(5-(adamantan-1-yl)-1,3,4-thiadiazol-2-yl)-2-

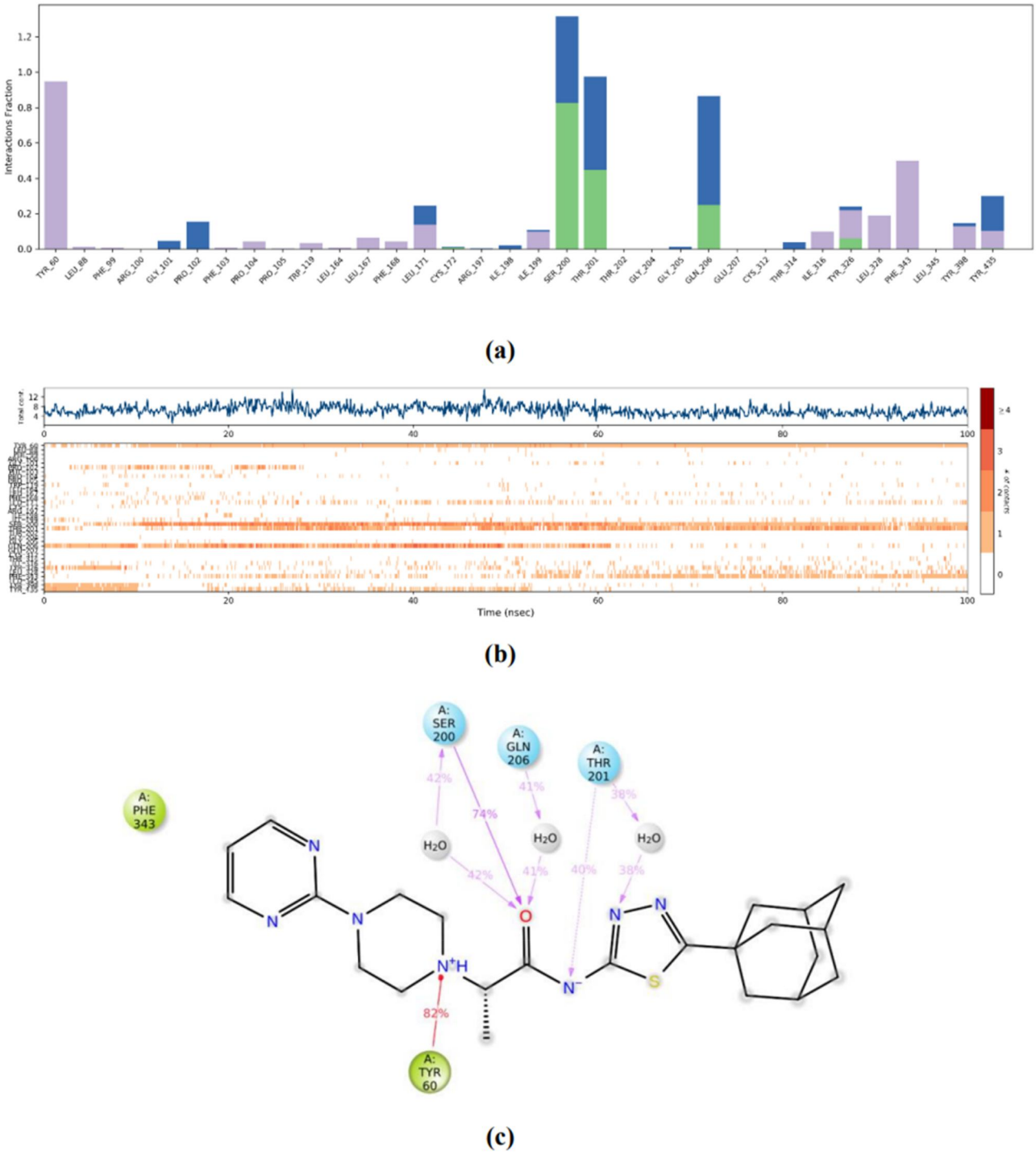

Figure 13. MDS studies of ligand **4a** within hMAO-B. The plots of (a) the interactions fraction-residue, (b) the residue-time and (c) the diagram of contact strength (cutoff = 30%) as 2D pose.

chloroacetamide **(2a)** (1.28 mmol, 0.4 g) were reacted in THF and TEA (1.54 mmol, 0.21 ml) for 12–24 hrs. After the reaction was completed, THF was first evaporated and solid residues were washed with water, filtered and recrystallized from ethanol.

N-[5-(adamantan-1-yl)-1,3,4-thiadiazol-2-yl]-2-(4-(pyrimidin-2-yl)piperazin-1-yl)acetamide (3a)

Yield: 96%. Physical appearance: light creamy powder. Experimental m.p.: 195–196 °C. IR (ATR) υ_{max} (cm^{-1}): 3153 (N–H stretching), 3030 (Aromatic sp^2 C–H stretching), 2926 – 2818 (sp^3 C–H stretching), 1695 (C = O stretching), 1583 – 1446 (aromatic C = C and C = N stretching), 1253 (C–N stretching). ^{1}H-NMR (300 MHz) (DMSO-d_6) δ (ppm): 1.73 (6H, s, adamantane-H), 1.99 (6H, s, adamantane-H), 2.04 (3H, s, adamantane-H), 2.55 (4H, t, J = 4.74 Hz, piperazine's $H_{2,6}$), 3.36 (2H, s, CO–CH_2), 3.75 (4H, t, J = 4.56 Hz, piperazine's $H_{3,5}$), 6.60 (1H, t, J = 7.74 Hz, pyrimidine's H_5), 8.34 (2H, d, J = 4.72 Hz, pyrimidine's $H_{4,6}$), 12.21 (1H, br-s, N–H). ^{13}C-NMR (75 MHz) (DMSO-d_6) δ (ppm): 28.29 (adamantane), 36.28 (adamantane), 37.66 (adamantane), 43.12 (adamantane), 43.66 (piperazine), 52.63 (piperazine), 60.47 (CO–$\underline{CH_2}$–), 110.55

(pyrimidine's C_5), 157.68 (thiadiazole), 158.37 (pyrimidyl's $C_{4,6}$), 161.6 (pyrimidine's C_2), 168.87 (thiadiazole), 174.11 (CO). HRMS (ESI) (*m/z*) $[M+1]^+$: for $C_{22}H_{29}N_7OS$ calculated: 440.2227; found: 440.2209.

N-[5-(adamantan-1-yl)-1,3,4-thiadiazol-2-yl]-2-(4-(pyridin-2-yl)piperazin-1- yl)acetamide (3b)

Yield: 81%. Physical appearance: light creamy powder. Experimental m.p.: 172–173 °C. IR (ATR) υ_{max} (cm^{-1}): 3151 (N–H stretching), 2927–2845 (sp^3 C–H stretching), 1701 (C = O stretching), 1591 – 1436 (aromatic C = C and C = N stretching), 1244 (C–N stretching). ^{1}H-NMR (300 MHz) (DMSO-d_6) δ (ppm): 1.73 (6H, s, adamantane-H), 1.99 (6H, s, adamantane-H), 2.04 (3H, s, adamantane-H), 2.59 (4H, br-s, piperazine's $H_{2,6}$), 3.37 (2H, s, CO–CH_2), 3.5 (4H, br-s, piperazine's $H_{3,5}$), 6.62 (1H, t, $J = 6.48$ Hz, pyridine's H_5), 6.8 (1H, d, $J = 8.58$ Hz, pyridine's H_3), 7.51 (1H, t, $J = 7.8$ Hz, pyridine's H_4), 8.09 (1H, d, $J = 4.77$ Hz, pyridine's H_6), 11.25 (H, br-s, N-H). ^{13}C-NMR (75 MHz) (DMSO-d_6) δ (ppm): 28.3 (adamantane), 36.28 (adamantane), 37.66 (adamantane), 43.12 (adamantane), 45.01 (piperazine), 52.64 (piperazine), 60.51 (CO–CH_2–), 107.54 (pyridine's C_3), 113.42 (pyridine's C_5), 137.95 (pyridine's C_4), 148 (pyridine's C_6), 157.7 (thiadiazole), 159.41 (pyridine's C_2), 168.86 (thiadiazole), 174.11 (CO). HRMS (ESI) (*m/z*) $[M+1]^+$: for $C_{23}H_{30}N_6OS$ calculated: 439.2275; found: 439.2263.

N-[5-(adamantan-1-yl)-1,3,4-thiadiazol-2-yl]-2-(4-phenylpiperazin-1-yl)acetamide (3c)

Yield: 94%. Physical appearance: light yellow powder. Experimental m.p.: 172–173 °C. IR (ATR) υ_{max} (cm^{-1}): 3142 (N–H stretching), 3022 (Aromatic sp^2 C–H stretching), 2904 – 2848 (sp^3 C-H stretching), 1687 (C = O stretching), 1597 – 1448 (aromatic C = C and C = N stretching), 1284 (C–N stretching). ^{1}H-NMR (300 MHz) (DMSO-d_6) δ (ppm): 1.73 (6H, s, adamantane-H), 1.98 (6H, s, adamantane-H), 2.03 (3H, s, adamantane-H), 2.65 (4H, br-s, piperazine's $H_{2,6}$), 3.14 (4H, br-s, piperazine's $H_{3,5}$), 3.37 (2H, s, CO–CH_2), 6.76 (1H, t, $J = 7.11$ Hz, phenyl H_4), 6.91 (2H, d, $J = 8.1$ Hz, phenyl $_{2,6}$) 7.19 (2H, t, $J = 7.23$ Hz, phenyl $H_{3,5}$), 11.6 (H, br-s, N–H). ^{13}C-NMR (75 MHz) (DMSO-d_6) δ (ppm): 28.31 (adamantane), 36.29 (adamantane), 37.66 (adamantane), 43.13 (adamantane), 48.61 (piperazine), 52.85 (piperazine), 60.46 (CO–CH_2), 115.88 (phenyl), 119.27 (phenyl), 129.36 (phenyl), 151.43 (phenyl's C_1), 157.71 (thiadiazole), 168.82 (thiadiazole), 174.09 (CO). HRMS (ESI) (*m/z*) $[M+1]^+$: for $C_{24}H_{31}N_5OS$ calculated: 438.2322; found: 438.2306.

N-[5-(adamantan-1-yl)-1,3,4-thiadiazol-2-yl]-2-(4-(furan-2-carbonyl)piperazin-1-yl)acetamide (3d)

Yield: 75%. Physical appearance: white powder. Experimental m.p.: 206–207 °C. IR (ATR) υ_{max} (cm^{-1}): 3136 (N–H stretching), 3116 (Aromatic sp^2 C–H stretching), 2933 – 2843 (sp^3 C–H stretching), 1701 (C = O stretching), 1620 (C = O stretching), 1556 – 1436 (aromatic C = C and C = N stretching), 1300 – 1280 (Aromatic C–O stretching), 1134 (C–N stretching). ^{1}H-NMR (300 MHz) (DMSO-d_6) δ (ppm): 1.73 (6H, s, adamantane's H), 1.98 (6H, s, adamantane-H), 2.03 (3H, s, adamantane-H), 2.57 (4H, br-s, piperazine's $H_{2,6}$), 3.38 (2H, s, CO–CH_2), 3.67 (4H, br-s, piperazine's $H_{3,5}$), 6.6 (H, t, $J = 1.52$ Hz, furan-H_4), 6.97 (H, d, $J = 2.68$ Hz, furan-H_3), 7.82 (H, s, furan-H_5), 12.3 (H, br-s, N–H). ^{13}C-NMR (75 MHz) (DMSO-d_6) δ (ppm): 28.29 (adamantane), 36.28 (adamantane), 37.66 (adamantane), 43.12 (adamantane), 52.84 (piperazine), 60.12 (CO–CH_2–), 111.74 (furan), 116.01 (furan), 145.17 (furan), 147.4 (furan), 157.67 (thiadiazole), 158.7 (piperazine-CO-furan), 168.8 (thiadiazole), 174.12 (NH–CO–CH_2). HRMS (ESI) (*m/z*) $[M+1]^+$: for $C_{23}H_{29}N_5O_3S$ calculated: 456.2064; found: 456.2054.

N-[5-(adamantan-1-yl)-1,3,4-thiadiazol-2-yl]-2-(4-ethylpiperazin-1-yl)acetamide (3e)

Yield: 58%. Physical appearance: white powder. Experimental m.p.: 152–153 °C. IR (ATR) υ_{max} (cm^{-1}): 3140 (N–H stretching), 2966 – 2806 (sp^3 C–H stretching), 1701 (C = O stretching), 1564 – 1438 (aromatic C = N stretching), 1172 (C–N stretching). ^{1}H-NMR (300 MHz) ($CDCl_3$) δ (ppm): 1.10 (3H, t, $J = 7.23$ Hz, CH_2–CH_3), 1.80 (6H, s, adamantane-H), 2.10 (9H, s, adamantane-H), 2.46 (2H, q, $J_1 = 7.23$ Hz, $J_2 = 14.41$ Hz, CH_2–CH_3), 2.55 (4H, br-s, piperazine's $H_{3,5}$), 2.67 (4H, t, $J = 3.98$ Hz, piperazine's $H_{2,6}$), 3.28 (2H, s, CO–CH_2),10.55 (H, br-s, N–H). ^{13}C-NMR (75 MHz) ($CDCl_3$) δ (ppm): 11.96 (CH_2–CH_3) 28.41 (adamantane), 36.39 (adamantane), 37.88 (adamantane), 43.22 (adamantane), 52.16 (CH_2–CH_3), 52.49 (piperazine), 53.65 (piperazine), 60.01 (CO–CH_2–), 157.21 (thiadiazole), 168.5 (thiadiazole), 175.98 (CO). HRMS (ESI) (*m/z*) $[M+1]^+$: for $C_{20}H_{31}N_5OS$ calculated: 390.2322; found: 390.2304.

N-[5-(adamantan-1-yl)-1,3,4-thiadiazol-2-yl]-2-(4-methylpiperazin-1- yl)acetamide (3f)

Yield: 55%. Physical appearance: white powder. Experimental m.p.: 170–171 °C. IR (ATR) υ_{max} (cm^{-1}): 3153 (N–H stretching), 2929 – 2777 (sp^3 C–H stretching), 1705 (C = O stretching), 1571-1438 (aromatic C = N stretching), 1172 (C–N stretching). ^{1}H-NMR (300 MHz) (DMSO-d_6) δ (ppm): 1.73 (6H, s, adamantane-H), 1.98 (6H, s, adamantane-H), 2.03 (3H, s, adamantane-H), 2.14 (3H, s, $–CH_3$), 2.31 (4H, br-s, piperazine's H), 2.49 (4H, t, $J = 1.68$ Hz, piperazine's H), 3.28 (2H, s, CO–CH_2),12.03 (H, br-s, N–H). ^{13}C-NMR (75 MHz) (DMSO-d_6) δ (ppm): 28.3 (adamantane), 36.29 (adamantane), 37.65 (adamantane), 43.12 (adamantane), 46.21 (CH_3), 52.83 (piperazine), 55.01 (piperazine), 60.5 (CO–CH_2–), 157.67 (thiadiazole), 168.87 (thiadiazole), 174.05 (CO). HRMS (ESI) (*m/z*) $[M+1]^+$: for $C_{19}H_{29}N_5OS$ calculated: 376.2166; found: 376.2156.

N-[5-(adamantan-1-yl)-1,3,4-thiadiazol-2-yl]-2-(pyrrolidin-1-yl)acetamide (3 g)

Yield: 84%. Physical appearance: light brown powder. Experimental m.p.: 160–161 °C. IR (ATR) υ_{max} (cm^{-1}): 3159 (N–H stretching), 2926 – 2794 (sp^3 C–H stretching), 1703 (C = O stretching), 1556 – 1448 (aromatic C = N stretching), 1301 (C–N stretching). ^{1}H-NMR (300 MHz) (DMSO-d_6) δ (ppm): 1.68 – 1.74 (10H, m, adamantane-H and pyrrolidine's $H_{3,4}$), 1.98 (6H, s, adamantane-H), 2.03 (3H, s, adamantane-H), 2.57

(4H, br-s, pyrrolidine's $H_{2,5}$), 3.41 (2H,s, CO-$\underline{CH_2}$), 11.4 (H, br-s, N-H). ^{13}C-NMR (75 MHz) (DMSO-d_6) δ (ppm): 23.85 (pyrrolidine's $C_{3,4}$), 28.31(adamantane), 36.29 (adamantane), 37.64 (adamantane), 43.13 (adamantane), 53.81 (pyrrolidine's $C_{2,5}$), 57.94 (CO–$\underline{CH_2}$), 157.91(thiadiazole), 169.29 (thiadiazole), 173.94 (CO). HRMS (ESI) (*m/z*) $[M+1]^+$: for $C_{18}H_{26}N_4OS$ calculated: 347.1900; found: 347.1887.

N-[5-(adamantan-1-yl)-1,3,4-thiadiazol-2-yl]-2-(piperidin-1-yl)acetamide (3h)

Yield: 88%. Physical appearance: light yellow crystals. Experimental m.p.: 169-170 °C. Literature m.p.: 200–202 °C (Wassel et al., 2021). IR (ATR) υ_{max} (cm^{-1}): 3145 (N–H stretching), 2937 – 2845 (sp^3 C–H stretching), 1699 (C = O stretching), 1548 – 1438 (aromatic C = N stretching), 1305 (C–N stretching). ^{1}H-NMR (300 MHz) (DMSO-d_6) δ (ppm): 1.33 – 1.39 (2H, m, piperidine's H_4), 1.46 – 1.54 (4H, m, piperidine's $H_{3,5}$), 1.73 (6H, s, adamantane-H), 1.98 (6H, s, adamantane-H), 2.04 (3H, s, adamantane-H), 2.44 (4H, t, $J = 4.68$ Hz, piperidine's $H_{2,6}$), 3.24 (2H, s, CO–CH_2), 11.83 (H, br-s, N-H). ^{13}C-NMR (75 MHz) (DMSO-d_6) δ (ppm): 23.96 (piperidine's C_4), 25.91 (piperidine's $C_{3,5}$), 28.3 (adamantane), 36.29 (adamantane), 37.65 (adamantane), 43.13 (adamantane), 54.16 (piperidine's $C_{2,6}$), 61.39 (CO–$\underline{CH_2}$), 157.74 (thiadiazole), 169.16 (thiadiazole), 174.03 (CO). HRMS (ESI) (*m/z*) $[M+1]^+$: for $C_{19}H_{28}N_4OS$ calculated: 361.2057; found: 361.2036.

N-[5-(adamantan-1-yl)-1,3,4-thiadiazol-2-yl]-2-morpholinoacetamide (3i)

Yield: 89%. Physical appearance: light yellow. Experimental m.p.: 206–207 °C. IR (ATR) υ_{max} (cm^{-1}): 3163 (N–H stretching), 2900 – 2845 (sp^3 C–H stretching), 1705 (C = O stretching), 1548 – 1444 (aromatic C = N stretching), 1301 (C–N stretching), 1112 (C–O stretching). ^{1}H-NMR (300 MHz) (DMSO-d_6) δ (ppm): 1.72 (6H, s, adamantane-H), 1.97 (6H, s, adamantane-H), 2.01 (3H, s, adamantane-H), 2.49 (4H, br-s, morpholine's $H_{3,5}$), 3.30 (2H, s, CO–CH_2), 3.57 (4H, br-s, morpholine's $H_{2,6}$), 12.00 (1H, br-s, N–H). ^{13}C-NMR (75 MHz) (DMSO-d_6) δ (ppm): 28.3 (adamantane), 36.28 (adamantane), 37.63 (adamantane), 43.12 (adamantane), 53.3 (morpholine's $C_{3,5}$), 60.75 (CO–$\underline{CH_2}$), 66.55 (morpholine's $C_{2,6}$), 157.66 (thiadiazole), 168.71 (thiadiazole), 174.04 (CO). HRMS (ESI) (*m/z*) $[M+1]^+$: for $C_{18}H_{26}N_4O_2S$ calculated: 363.1849; found: 363.1831.

N-[5-(adamantan-1-yl)-1,3,4-thiadiazol-2-yl]-2-thiomorpholinoacetamide (3j)

Yield: 89%. Physical appearance: light brown. Experimental m.p.: 196–197 °C. IR (ATR) υ_{max} (cm^{-1}): 3172 (N–H stretching), 2931 – 2846 (sp^3 C–H stretching), 1703 (C = O stretching), 1517 – 1452 (aromatic C = N stretching), 1300 – 1286 (C–N stretching). ^{1}H-NMR (300 MHz) (DMSO-d_6) δ (ppm): 1.72 (6H, s, adamantane's $H_{6,8,9}$), 1.97 (6H, s, adamantane-H), 2.02 (3H, s, adamantane-H), 2.60 (4H, br-s, thiomorpholine's $H_{2,6}$), 2.73 (4H, br-s, thiomorpholine-$H_{3,5}$), 3.32 (2H, s, CO–CH_2), 11.88 (H, br-s, N–H). ^{13}C-NMR (75 MHz) (DMSO-d_6) δ (ppm): 27.95 (thiomorpholine's $C_{2,6}$), 28.7 (adamantane), 36.69 (adamantane), 38.07 (adamantane), 43.53 (adamantane), 54.95 (thiomorpholine's $C_{3,5}$), 61.61 (CO–$\underline{CH_2}$), 158.06 (thiadiazole), 169.53 (thiadiazole), 174.51 (CO). HRMS (ESI) (*m/z*) $[M+1]^+$: for $C_{18}H_{26}N_4OS_2$ calculated: 379.1621; found: 379.1611.

General synthesis of N-[5-(adamantan-1-yl)-1,3,4-thiadiazol-2-yl]-2-substituted-propanamide derivatives (4a–4g)

Using reflux, an appropriate cyclic secondary amine (1.23 mmol) and *N*-[5-(adamantan-1-yl)-1,3,4-thiadiazol-2-yl]-2-chloropropanamide **(2b)** (1.23 mmol, 0.4 g) were reacted in acetonitrile and K_2CO_3 (2.46 mmol, 0.34 g) for 12–24 hrs. After the reaction was completed, THF was first evaporated, solid residues were washed with water, filtered and recrystallized from ethanol while liquid residue was extracted using ethyl acetate.

N-[5-(adamantan-1-yl)-1,3,4-thiadiazol-2-yl]-2-(4-(pyrimidin-2-yl)piperazin-1-yl)propanamide (4a)

Yield: 67%. Physical appearance: white powder. Experimental m.p.: 115–116 °C. IR (ATR) υ_{max} (cm^{-1}): 3149 (N–H stretching), 2902 – 2848 (sp^3 C–H stretching), 1695 (C = O stretching), 1585 – 1446 (aromatic C = C and C = N stretching), 1163 (C–N stretching). ^{1}H-NMR (300 MHz) (DMSO-d_6) δ (ppm): 1.20 (3H, br-s, CH–$\underline{CH_3}$), 1.71 (6H, s, adamantane-H), 1.97 (6H, adamantane-H), 2.01 (3H, s, adamantane-H), 2.55 (4H, br-s, piperazine's $H_{2,6}$), 3.56 (1H, q, $J_1 = 5.41$ Hz, $J_2 = 10.56$ Hz, $\underline{CH}$–CH_3), 3.72 (4H,s, piperazine-$H_{3,5}$), 6.59 (1H, t, $J = 4.05$ Hz, pyrimidine's H_5), 8.31 (2H, br-s, pyrimidine's $H_{4,6}$), 12.64 (H, br-s, N-H). ^{13}C-NMR (75 MHz) (DMSO-d_6) δ (ppm): 13.83 (CH–$\underline{CH_3}$), 28.74 (adamantane), 36.74 (adamantane), 38.07 (adamantane), 43.57 (adamantane), 44.43 (piperazine), 49.57 (piperazine), 62.73 (CO–$\underline{CH}$), 110.91 (pyrimidine), 158.35 (thiadiazole), 158.78 (pyrimidine), 161.98 (pyrimidine), 171.93 (thiadiazole), 174.45 (CO). HRMS (ESI) (*m/z*) $[M+1]^+$: for $C_{23}H_{31}N_7OS$ calculated: 454.2384; found: 454.2362.

N-[5-(adamantan-1-yl)-1,3,4-thiadiazol-2-yl]-2-(4-(pyridin-2-yl)piperazin-1- yl)propanamide (4b)

Yield: 72%. Physical appearance: white powder. Experimental m.p.: 240–241 °C. IR (ATR) υ_{max} (cm^{-1}): 3001 (N–H stretching), 2902 – 2821 (sp^3 C–H stretching), 1697 or 1591 (C = O stretching), 1554 – 1435 (aromatic C = C and C = N stretching), 1242 (C–N stretching). ^{1}H-NMR (300 MHz) (DMSO-d_6) δ (ppm): 1.18 (3H, d, $J = 6.73$ Hz, –CH–$\underline{CH_3}$), 1.72 (6H, s, adamantane-H), 1.95 (6H, s, adamantane-H), 2.01 (3H, s, adamantane-H), 2.58 (4H, t, $J = 6.15$ Hz, piperazine's $H_{2,6}$), 3.30 (1H, q, $J_1 = 6.59$ Hz, $J_2 = 14.38$ Hz, $\underline{CH}$–CH_3), 3.43 (4H, s, piperazine's $H_{3,5}$), 6.59 (H, t, $J = 5.87$ Hz, pyridine's H_5), 6.77 (H, d, $J = 8.56$ Hz, pyridine's H_3), 7.48 (H, t, $J = 6.91$ Hz, pyridine's H_4), 8.07 (H, d, $J = 4.53$ Hz, pyridine's H_6). ^{13}C-NMR (75 MHz) (DMSO-d_6) δ (ppm): 15.02 (CH–$\underline{CH_3}$), 28.41 (adamantane), 36.53 (adamantane), 37.5 (adamantane), 43.31 (adamantane), 45.45 (piperazine), 49.47 (piperazine), 64.62 (CO–$\underline{CH}$), 107.42 (pyridine), 113.21 (pyridine), 137.86 (pyridine), 147.98 (pyridine), 159.53 (thiadiazole), 163.48 (pyridine), 171.37

(thiadiazole), 174.3 (CO). HRMS (ESI) (*m/z*) $[M+1]^+$: for $C_{24}H_{32}N_6OS$ calculated: 453.2431; found: 453.2417.

N-[5-(adamantan-1-yl)-1,3,4-thiadiazol-2-yl]-2-(4-phenylpiperazin-1-yl) propanamide (4c)

Yield: 74%. Physical appearance: light creamy powder. Experimental m.p.: 241–242 °C. IR (ATR) υ_{max} (cm^{-1}): 3061 (N–H stretching), 2904 – 2848 (sp^3 C–H stretching), 1697 (C = O stretching), 1552 – 1504 (aromatic C = C and C = N stretching), 1282 (C–N stretching). ^{1}H-NMR (400 MHz) ($CDCl_3$) δ (ppm): 1.40 (3H, d, J = 6.98 Hz, COCH–$\underline{CH_3}$), 1.81 (6H, s, adamantane-H), 2.12 (9H, s, adamantane-H), 2.71 – 2.83 (4H, m, piperazine-H), 3.05 and 3.16 (2H, 2t, J = 4.77 Hz and J = 4.69 Hz, piperazine-H), 3.28 (2H, br-s, piperazine-H), 3.48 (1H, q, J_1 = 6.98 Hz, J_2 = 13.98 Hz, CO$\underline{CH}$–CH_3), 6.89 (1H, t, J = 6.04 Hz, phenyl's H_4), 6.95 (2H, d, J = 8.13 Hz, phenyl's $H_{2,6}$), 7.29 (2H, t, J = 7.72 Hz, phenyl's $H_{3,5}$). ^{13}C-NMR (100 MHz) ($CDCl_3$) δ (ppm): 10.97 (COCH–$\underline{CH_3}$), 28.43 (adamantane), 36.41 (adamantane), 37.89 (adamantane), 43.24 (adamantane), 49.49 (piperazine), 49.79 (piperazine), 63.71 (CO–$\underline{CH}$), 116.41 (phenyl), 120.24 (phenyl), 129.20 (phenyl), 150.98 (phenyl), 157.57 (thiadiazole), 171.73 (thiadiazole), 175.87 (CO). HRMS (ESI) (*m/z*) $[M+1]^+$: for $C_{25}H_{33}N_5OS$ calculated: 452.2479; found: 452.2462.

N-[5-(adamantan-1-yl)-1,3,4-thiadiazol-2-yl]-2-(4-ethylpiperazin-1-yl) propanamide (4d)

Yield: 50%. Physical appearance: white powder. Experimental m.p.: 99–100 °C. IR (ATR) υ_{max} (cm^{-1}): 3157 (N–H stretching), 2904 – 2819 (sp^3 C–H stretching), 1699 (C = O stretching), 1508 – 1450 (aromatic C = N stretching), 1170 (C–N stretching). ^{1}H-NMR (300 MHz) (DMSO-d_6) δ (ppm): 0.94 (3H, t, J = 7.02 Hz, N–$CH_2\underline{CH_3}$), 1.17 (3H, d, J = 6.71 Hz, CO–CH–$\underline{CH_3}$), 1.73 (6H, s, adamantane-H), 1.98 (6H, s, adamantane-H), 2.03 (3H, s, adamantane-H), 2.22–2.33 (10H, m, piperazine's H and N–$\underline{CH_2}$–CH_3), 3.47 (1H, q, J_1= 6.58 Hz, J_2= 13.29 Hz, $\underline{CH}$–CH_3), 12.06 (1H, br-s, N-H). ^{13}C-NMR (75 MHz) (DMSO-d_6) δ (ppm): 12.49 (N–$CH_2\underline{CH_3}$), 13.33 (CO–CH–$\underline{CH_3}$), 28.29 (adamantane), 36.29 (adamantane), 37.64 (adamantane), 43.13 (adamantane), 49.19 (N–$\underline{CH_2}CH_3$), 52.04 (piperazine), 53.06 (piperazine), 62.14 (CO-$\underline{CH}$), 157.71(thiadiazole), 171.42 (thiadiazole), 174.06 (CO). HRMS (ESI) (*m/z*) $[M+1]^+$: for $C_{21}H_{33}N_5OS$ calculated: 404.2479; found: 404.2467.

N-[5-(adamantan-1-yl)-1,3,4-thiadiazol-2-yl]-2-(4-(2-(dimethylamino)ethyl) piperazin-1-yl)propanamide (4e)

Yield: 73%. Physical appearance: light yellow liquid. IR (ATR) υ_{max} (cm^{-1}): 3145 (N–H stretching), 2900 – 2816 (sp^3 C–H stretching), 1693 (C = O stretching), 1514 – 1290 (aromatic C = N stretching), 1165 – 1014 (C–N stretching). ^{1}H-NMR (300 MHz) (DMSO-d_6) δ (ppm): 1.14 – 1.20 (3H, m, COCH–$\underline{CH_3}$), 1.74 (6H, s, adamantane-H), 1.99 (6H, adamantane-H), 2.04 (3H, s, adamantane-H), 2.12 (6H, s, N–$(CH_3)_2$), 2.32 (4H, br-s, piperazine- H), 2.38 (4H, br-s, piperazine-H), 2.95–3.35 (2H, m, N–CH_2), 3.47 (2H,q, J_1 = 6.72 Hz, J_2 = 13.53 Hz, N–CH_2), 4.03 (1H,q, J_1 = 7.11 Hz, J_2 = 14.25 Hz, CO–$\underline{CH}$–CH_3). ^{13}C-NMR (75 MHz) (DMSO-d_6) δ (ppm): 13.34 (COCH–$\underline{CH_3}$), 28.29 (adamantane), 36.29 (adamantane), 37.64 (adamantane), 43.12 (adamantane), 45.92 (N–$(CH_3)_2$), 49.18 (piperazine), 53.78 (piperazine), 56.23 (piperazine–$(CH_2)_2$–N), 56.94 (piperazine–$(CH_2)_2$–N), 62.09 (CO–$\underline{CH}$), 157.66 (thiadiazole), 171.37 (thiadiazole), 174.08 (CO). HRMS (ESI) (*m/z*) $[M+1]^+$: For $C_{23}H_{38}N_6OS$ calculated: 447.2901; found: 447.2880.

N-[5-(adamantan-1-yl)-1,3,4-thiadiazol-2-yl]-2-(pyrrolidin-1-yl)propanamide (4f)

Yield: 70%. Physical appearance: white powder. Experimental m.p.: 158–159 °C. IR (ATR) υ_{max} (cm^{-1}): 3134 (N–H stretching), 2974 – 2794 (sp^3 C–H stretching), 1691 (C = O stretching), 1537 – 1450 (aromatic C = N stretching), 1294 (C–N stretching). ^{1}H-NMR (400 MHz) ($CDCl_3$) δ (ppm): 1.39 (3H, d, J = 7.01 Hz, COCH–$\underline{CH_3}$), 1.80 (6H, s, adamantane-H), 1.83 – 1.88 (4H, m, pyrrolidine's $H_{3,4}$), 2.11 (9H, s, adamantane-H), 2.60–2.69 (4H, m, pyrrolidine's $H_{2,5}$), 3.30 (1H, q, J_1 = 6.99 Hz, J_2 = 13.98 Hz, CO$\underline{CH}$–CH_3). ^{13}C-NMR (100 MHz) ($CDCl_3$) δ (ppm): 15.40 (COCH–$\underline{CH_3}$), 23.47 (pyrrolidine's $C_{3,4}$), 28.44 (adamantane), 36.41 (adamantane), 37.86 (adamantane), 43.23 (adamantane), 50.88 (pyrrolidine's $C_{2,5}$), 62.43 (CO–$\underline{CH}$), 157.6 (thiadiazole), 172.86 (thiadiazole), 175.77 (CO). HRMS (ESI) (*m/z*) $[M+1]^+$: for $C_{19}H_{28}N_4OS$ calculated: 361.2057; found: 361.2042.

N-[5-(adamantan-1-yl)-1,3,4-thiadiazol-2-yl]-2-morpholinopropanamide (4 g)

Yield: 63%. Physical appearance: white powder. Experimental m.p.: 195–196 °C. IR (ATR) υ_{max} (cm^{-1}): 3161 (N–H stretching), 2927 – 2852 (sp^3 C–H stretching), 1734 (C = O stretching), 1541 – 1448 (aromatic C = N stretching), 1296 (C–N stretching), 1116 (C–O stretching). ^{1}H-NMR (300 MHz) (DMSO-d_6) δ (ppm): 1.19 (3H, d, J = 6.81 Hz, COCH–$\underline{CH_3}$), 1.74 (6H, s, adamantane-H), 1.99 (6H, s, adamantane-H), 2.04 (3H, s, adamantane-H), 2.43–2.55 (4H, m, morpholine's $H_{3,5}$), 3.48 (1H, q, J_1 = 6.87 Hz, J_2 = 13.75 Hz, CO–$\underline{CH}$), 3.57 (4H, s, morpholine's $H_{2,6}$), 12.17 (1H, br-s, N-H). ^{13}C-NMR (75 MHz) (DMSO-d_6) δ (ppm): 13.29 (COCH–$\underline{CH_3}$), 28.29 (adamantane), 36.29 (adamantane), 37.64 (adamantane), 43.12 (adamantane), 49.8 (morpholine $C_{3,5}$), 62.4 (morpholine $C_{2,6}$), 66.85 (CO–$\underline{CH}$), 157.67 (thiadiazole), 171.34 (thiadiazole), 174.13 (CO). HRMS (ESI) (*m/z*) $[M+1]^+$: for $C_{19}H_{28}N_4O_2S$ calculated: 337.2006; found: 337.1987.

In-vitro enzyme studies

AChE inhibitions

Anticholinesterase activity of the synthesized derivatives was *in vitro* evaluated against AChE (E.C.3.1.1.7, electric eel) and BChE (BChE-E.C.3.1.1.8, horse serum) using the reference drugs donepezil and tacrine, respectively. A modified Ellman's method as reported previously (Ellman et al., 1961; Sağlık et al., 2016) was used. This method depends on the measurement of a yellow-colored chromophore that produces upon the reaction of 5,5-dithiobis (2-nitrobenzoic acid) (DTNB) with thiocholines produced from substrates, acetylthiocholine iodide (ATC) or butyrylthiocholine iodide (BTC), hydrolysis by

cholinesterase enzymes. Inhibitor solutions of derivatives **3a–3j**, **4a–4g**, donepezil and tacrine were prepared in 2% DMSO at initial concentrations of 10^{-3} and 10^{-4} M. In 96-well plates, 2.5 U/ml AChE or BChE enzyme solution (20 µl/well), phosphate buffer (140 µl/well), inhibitor solution (20 µl/well), 0.01 M DTNB solution (20 µl/well) and 0.075 M ATC or BTC solution (10 µl/well) were all mixed and incubated at 25 °C for 15 mins. A blank,without inhibitor and substrate solution, and a negative control,without inhibitor solution, were also prepared. Absorbances of the yellow-colored chromophore were measured twice at 412 nm over 5 mins intervals using a microplate reader (BioTek-Synergy H1, USA). The experiment was done quadrat. The same process was performed at lower concentrations from 10^{-5} to 10^{-9} M for derivatives that displayed over 50% inhibition activity at the initial concentrations and for reference drugs to calculate their IC_{50} values . Data are presented as mean ± standard deviation (SD). The inhibition % was determined using the following equation,

$$\frac{\left[\left(A(C)-A(B)\right)-\left(A(I)-A(B)\right)\right]}{\left(A\ (C)-A(B)\right)}\ \times\ 100,$$

B: blank, C: control, A(B): difference in absorbance readings of the blank sample, A(C): difference in absorbance readings of the control sample and A(I): difference in absorbance readings of the inhibitor sample. Dose-response curves represented as inhibition % vs. log concentrations using the GraphPad 'PRISM' software (version 5.0) were plotted to calculate IC_{50} values.

MAO inhibitions

MAO inhibition activity of the synthesized derivatives was evaluated against both *h*MAO-A and *h*MAO-B using the reference drugs moclobemide and selegiline, respectively by using *in vitro* Ampliflu™ Red-based fluorimetric assay (Sağlık et al., 2019) which depends on the detection of hydrogen peroxides generated by both subtypes of MAO enzymes during tyramine's oxidation that further react with Ampliflu™ Red non-fluorescent agent in the presence of horseradish peroxidase to give the measurable fluorescent resorufin substance. Inhibitor solutions of derivatives **3a–3j**, **4a–4g**, moclobemide and selegiline were prepared in 2% DMSO at initial concentrations of 10^{-3} and 10^{-4} M. In a black flat-bottomed 96-well plate, 0.5 U/ml *h*MAO-A or 0.64 U/ml *h*MAO-B (100 µl/well) and inhibitor solution (20 µl/well) were mixed and incubated at 37 °C for 30 mins. Then, 100 µl/well of the working solution (the fluorescence reagent Ampliflu™ Red (20 mM, 200 µl), Horseradish peroxidase (200 U/ml, 100 µl) and tyramine (100 mM, 200 µl)) was added and incubated at 37 °C for another 30 mins. Resorufin level was measured on the fluorescence (Ex/Em: 535/587 nm) at 5-mins intervals. Besides that, the following samples were prepared: negative control by replacing inhibitor solution with 2% DMSO); blank sample by replacing *h*MAO isoforms with phosphate buffer to measure the background activity; another sample by replacing enzyme solutions with 3% H_2O_2 solution to assess each inhibitor's ability to inhibit horseradish peroxidase and samples containing only working and inhibitor solutions to assess each inhibitor's ability to affect the produced fluorescence due to non-enzymatic inhibition. The experiment was done four times. The same process was repeated at lower concentrations from 10^{-5} to 10^{-9} M for derivatives that displayed over 50% inhibition activity at the initial concentrations and for reference drugs to determine their IC_{50} values. Data are presented as mean ± standard deviation (SD). The % inhibition was calculated using the equation shown below after subtracting the background activity to calculate the specific fluorescence emission value for each compound.

$$\frac{(FC_{t2}\ -\ FC_{t1})-\ (FI_{t2}\ -\ FI_{t1})}{FC_{t2}\ -\ FC_{t1}}\ \times\ 100,$$

FCt_2: fluorescence of the control sample measured at t_2 time, FCt_1: fluorescence of the control sample measured at t_1 time, Flt_2: fluorescence of an inhibitor sample measured at t_2 time, Flt1: fluorescence of an inhibitor sample measured at t_1 time.

Dose-response curves represented as inhibition % vs. log concentrations using the GraphPad 'PRISM' software (version 5.0) were plotted to calculate IC_{50} values.

In-silico studies

Pharmacokinetic properties prediction

Nowadays, many *in silico* programs have been established to give an earlier prediction of the safety and efficacy of drug candidates depending on their physiochemical properties, hence pharmacokinetic properties. ADME parameters of the most active derivatives (**3a**, **3b**, **3d**, **4a** and **4b**) and the reference drugs (donepezil and selegiline) were estimated using both SwissADME and Molsoft.

Molecular docking studies

The binding interactions within *h*AChE and *h*MAO-B of the most active derivatives **4a**, **4b**, **3a** and **4a**, respectively were visualized using the *in-silico* Schrödinger Maestro interface (Schrödinger, 2020). The X-ray crystal structures of *h*AChE (PDB ID: *4EY7*) and *h*MAO-B (PDB ID: *2V5Z*) were first imported from the Protein Data Bank server (www.rcsb.org), then the Protein Preparation Wizard protocol of the Schrödinger Suite 2020 was applied to prepare enzymes for docking, while LigPrep module (Schrödinger, 2020) was applied to prepare the ligands with their proper atom types and the protonation states at pH 7.4 ± 1.0. In addition to that, hydrogen atoms and bond orders were further inserted into the structures. The grid and docking simulations were conducted in standard precision docking mode using the Glide module (Schrödinger, 2020).

Molecular dynamic simulation (MDS) studies

The nature of the binding interactions as well as the time-dependent stability of a ligand-target complex was evaluated using MDS studies that were run for 100 ns (100 trajectory and 1000 frames, NPγT condition) at 310.55 K (body temperature) according to standard procedure (Evren et al., 2022; Sağlık et al., 2022; Turan Yücel et al., 2022). The Desmond program

(Schrödinger, 2020) was run by applying the standard force field (OPLS3e) of the Schrödinger Suite with a transferable intermolecular potential with a 3-points (TIP3P) water model then an energy minimization of the complex was applied (Sureshkumar et al., 2018). Both Na^+ and Cl^- ions were used for system neutralization. MDS studies were performed after the system setup was completed. The Rg, RMSD and RMSF values were calculated by the Desmond program (Schrödinger, 2020).

Conclusion

With the scope of developing MTD for AD, different derivatives of *N*-[5-(adamantan-1-yl)-1,3,4-thiadiazol-2-yl]-2-(4-un/substituted) cyclic secondary amino-acetamide/propanamide were synthesized and evaluated *in vitro* against AChE, BChE, *h*-MAO-A and *h*-MAO-B that are pathological targets in AD. Generally, derivatives were selective inhibitors toward AChE and *h*-MAO-B. Derivatives **4a**, **4b** and **3a** ordered from the most active to the least displayed dual inhibition activity against both AChE and *h*-MAO-B, however derivatives **3d** and **3b** displayed significant inhibition activity against only AChE.

In terms of SAR, the piperazine ring, the methyl group within the propanamide skeleton and the aromatic pyrimidine ring at the fourth position of piperazine were all noticed to have a more favorable impact on the inhibitory activity.

In terms of binding within the enzyme's active site, all derivatives that showed inhibition activity against AChE were found to bind both CAS and PAS of the enzyme which highlights the potential ability of these derivatives to block the generation of the neurotoxic AChE- Aβ complexes. Interestingly, maintaining balanced interactions with Trp86 and His447 beside the other common binding interactions was noticed to be the ideal situation for activity against AChE, however, the absence of binding with Trp86 leads to a more decrement in activity compared to the absence of His447. On the other hand, binding interactions with Gln 206 are considered important for selectivity against *h*MAO-B. Binding interactions with FAD within the active site were also among the positive contributors to the activity against *h*MAO-B.

Acknowledgments

As this paper is a part of a Master's Thesis, the authors gratefully acknowledge the support of both DOPNA Laboratory and AÜ-BİBAM Laboratory.

Disclosure statement

No potential conflict of interest was reported by the authors.

Funding

The author(s) reported there is no funding associated with the work featured in this article.

ORCID

Amal A. AL-Sharabi http://orcid.org/0000-0002-9745-0838
Asaf Evrim Evren http://orcid.org/0000-0002-8651-826X
Begüm Nurpelin Sağlık http://orcid.org/0000-0002-0151-6266
Leyla Yurttaş http://orcid.org/0000-0002-0957-6044

References

Abeysinghe, A., Deshapriya, R., & Udawatte, C. (2020). Alzheimer's disease; a review of the pathophysiological basis and therapeutic interventions. *Life Sciences*, *256*, 117996. https://doi.org/10.1016/j.lfs.2020.117996

Aliabadi, A. (2016). 1,3,4-Thiadiazole Based Anticancer Agents. *Anti-Cancer Agents in Medicinal Chemistry*, *16*(10), 1301–1314. https://doi.org/10.2174/1871520616666160628100936

Alvarez, A., Opazo, C., Alarcon, R., Garrido, J., & Inestrosa, N. C. (1997). Acetylcholinesterase promotes the aggregation of amyloid-beta-peptide fragments by forming a complex with the growing fibrils. *Journal of Molecular Biology*, *272*(3), 348–361. https://doi.org/10.1006/jmbi.1997.1245

Bartus, R. T., Dean, R. L., 3rd, Beer, B., & Lippa, A. S. (1982). The cholinergic hypothesis of geriatric memory dysfunction. *Science (New York, N.Y.)*, *217*(4558), 408–414. https://doi.org/10.1126/science.7046051

Can, Ö. D., Osmaniye, D., Demir Özkay, Ü., Sağlık, B. N., Levent, S., Ilgın, S., Baysal, M., Özkay, Y., & Kaplancıklı, Z. A. (2017). MAO enzymes inhibitory activity of new benzimidazole derivatives including hydrazone and propargyl side chains. *European Journal of Medicinal Chemistry*, *131*, 92–106. https://doi.org/10.1016/j.ejmech.2017.03.009

Çavuşoğlu, B. K., Sağlık, B. N., Özkay, Y., İnci, B., & Kaplancıklı, Z. A. (2018). Design, synthesis, monoamine oxidase inhibition and docking studies of new dithiocarbamate derivatives bearing benzylamine moiety. *Bioorganic Chemistry*, *76*, 177–187. https://doi.org/10.1016/j.bioorg.2017.11.012

Cheung, J., Rudolph, M. J., Burshteyn, F., Cassidy, M. S., Gary, E. N., Love, J., Franklin, M. C., & Height, J. J. (2012). Structures of human acetylcholinesterase in complex with pharmacologically important ligands. *Journal of Medicinal Chemistry*, *55*(22), 10282–10286. https://doi.org/10.1021/jm300871x

Daina, A., Michielin, O., & Zoete, V. (2017). SwissADME: A free web tool to evaluate pharmacokinetics, drug-likeness and medicinal chemistry friendliness of small molecules. *Scientific Reports*, *7*(1), 42717. https://doi.org/10.1038/srep42717

Dawood, K. M., & Farghaly, T. A. (2017). Thiadiazole inhibitors: A patent review. *Expert Opinion on Therapeutic Patents*, *27*(4), 477–505. https://doi.org/10.1080/13543776.2017.1272575

Drug-likeness and molecular property prediction. Molsoft L.L.C.

Ellman, G. L., Courtney, K. D., Andres, V., & Feather-Stone, R. M. (1961). A new and rapid colorimetric determination of acetylcholinesterase activity. *Biochemical Pharmacology*, *7*(2), 88–95. https://doi.org/10.1016/0006-2952(61)90145-9

Evren, A. E., Nuha, D., Dawbaa, S., Sağlık, B. N., & Yurttaş, L. (2022). Synthesis of novel thiazolyl hydrazone derivatives as potent dual monoamine oxidase-aromatase inhibitors. *European Journal of Medicinal Chemistry*, *229*, 114097. https://doi.org/10.1016/j.ejmech.2021.114097

Ferris, S. H. (2003). Evaluation of memantine for the treatment of Alzheimer's disease. *Expert Opinion on Pharmacotherapy*, *4*(12), 2305–2313. https://doi.org/10.1517/14656566.4.12.2305

Fesatidou, M., Zagaliotis, P., Camoutsis, C., Petrou, A., Eleftheriou, P., Tratrat, C., Haroun, M., Geronikaki, A., Ciric, A., & Sokovic, M. (2018). 5-Adamantan thiadiazole-based thiazolidinones as antimicrobial agents. Design, synthesis, molecular docking and evaluation. *Bioorganic & Medicinal Chemistry*, *26*(16), 4664–4676. https://doi.org/10.1016/j.bmc.2018.08.004

Gauthier, S., José, P. R.-N., Morais, A., & Webster, C. (2021). *World Alzheimer report 2021: Journey through the diagnosis of dementia*.

Guzior, N., Wieckowska, A., Panek, D., & Malawska, B. (2015). Recent development of multifunctional agents as potential drug candidates

for the treatment of Alzheimer's disease. *Current Medicinal Chemistry*, *22*(3), 373–404. https://doi.org/10.2174/0929867321666141106122628

Haddad, H. W., Malone, G. W., Comardelle, N. J., Degueure, A. E., Kaye, A. M., & Kaye, A. D. (2022). Aducanumab, a novel anti-amyloid monoclonal antibody, for the treatment of Alzheimer's disease: A comprehensive review. *Health Psychology Research*, *10*(1), 31925. https://doi.org/10.52965/001c.31925

Haider, S., Alam, M. S., & Hamid, H. (2015). 1,3,4-Thiadiazoles: A potent multi targeted pharmacological scaffold. *European Journal of Medicinal Chemistry*, *92*, 156–177. https://doi.org/10.1016/j.ejmech.2014.12.035

Han, X., Yu, Y. L., Hu, Y. S., & Liu, X. H. (2021). 1,3,4-thiadiazole: A privileged scaffold for drug design and development. *Current Topics in Medicinal Chemistry*, *21*(28), 2546–2573. https://doi.org/10.2174/1568026621666211111154342

Hiremathad, A., & Piemontese, L. (2017). Heterocyclic compounds as key structures for the interaction with old and new targets in Alzheimer's disease therapy. *Neural Regeneration Research*, *12*(8), 1256–1261. https://doi.org/10.4103/1673-5374.213541

Jain, A. K., Sharma, S., Vaidya, A., Ravichandran, V., & Agrawal, R. K. (2013). 1,3,4-thiadiazole and its derivatives: A review on recent progress in biological activities. *Chemical Biology & Drug Design*, *81*(5), 557–576. https://doi.org/10.1111/cbdd.12125

Joseph, L., George, M., & Mathews, P. (2015). A review on various biological activities of 1, 3, 4-thiadiazole derivatives. *Journal of Pharmaceutical Chemical and Biological Sciences*, *3*(1), 329–345.

Kaya, B., Sağlık, B. N., Levent, S., Özkay, Y., & Kaplancıklı, Z. A. (2016). Synthesis of some novel 2-substituted benzothiazole derivatives containing benzylamine moiety as monoamine oxidase inhibitory agents. *Journal of Enzyme Inhibition and Medicinal Chemistry*, *31*(6), 1654–1661. https://doi.org/10.3109/14756366.2016.1161621

Kumar, N., Kumar, V., Anand, P., Kumar, V., Ranjan Dwivedi, A., & Kumar, V. (2022). Advancements in the development of multi-target directed ligands for the treatment of Alzheimer's disease. *Bioorganic & Medicinal Chemistry*, *61*, 116742. https://doi.org/10.1016/j.bmc.2022.116742

Lamoureux, G., & Artavia, G. (2010). Use of the adamantane structure in medicinal chemistry. *Current Medicinal Chemistry*, *17*(26), 2967–2978. https://doi.org/10.2174/092986710792065027

Li, Y., Geng, J., Liu, Y., Yu, S., & Zhao, G. (2013). Thiadiazole-a promising structure in medicinal chemistry. *ChemMedChem*. *8*(1), 27–41. https://doi.org/10.1002/cmdc.201200355

Manzoor, S., & Hoda, N. (2020). A comprehensive review of monoamine oxidase inhibitors as Anti-Alzheimer's disease agents: A review. *European Journal of Medicinal Chemistry*, *206*, 112787. https://doi.org/10.1016/j.ejmech.2020.112787

Martorana, A., Giacalone, V., Bonsignore, R., Pace, A., Gentile, C., Pibiri, I., Buscemi, S., Lauria, A., & Piccionello, A. P. (2016). Heterocyclic Scaffolds for the Treatment of Alzheimer's Disease. *Current Pharmaceutical Design*, *22*(26), 3971–3995. https://doi.org/10.2174/1381612822666160518141650

Marucci, G., Buccioni, M., Ben, D. D., Lambertucci, C., Volpini, R., & Amenta, F. (2021). Efficacy of acetylcholinesterase inhibitors in Alzheimer's disease. *Neuropharmacology*, *190*, 108352. https://doi.org/10.1016/j.neuropharm.2020.108352

Massoud, F., & Leger, G. C. (2011). Pharmacological treatment of Alzheimer disease. *The Canadian Journal of Psychiatry*, *56*(10), 579–588. https://doi.org/10.1177/070674371105601003

Patani, G. A., & LaVoie, E. J. (1996). Bioisosterism: A rational approach in drug design. *Chemical Reviews*, *96*(8), 3147–3176. https://doi.org/10.1021/cr950066q

Sağlık, B. N., Ilgın, S., & Özkay, Y. (2016). Synthesis of new donepezil analogues and investigation of their effects on cholinesterase enzymes. *European Journal of Medicinal Chemistry*. *124*, 1026–1040. https://doi.org/10.1016/j.ejmech.2016.10.042

Sağlık, B. N., Kaya Çavuşoğlu, B., Osmaniye, D., Levent, S., Acar Çevik, U., Ilgın, S., Özkay, Y., Kaplancıklı, Z. A., & Öztürk, Y. (2019). In vitro and in silico evaluation of new thiazole compounds as monoamine oxidase inhibitors. *Bioorganic Chemistry*, *85*, 97–108. https://doi.org/10.1016/j.bioorg.2018.12.019

Sağlık, B. N., Levent, S., Osmaniye, D., Evren, A. E., Karaduman, A. B., Özkay, Y., & Kaplancıklı, Z. A. (2022). Design, synthesis, and in vitro and in silico approaches of novel indanone derivatives as multifunctional anti-Alzheimer agents. *ACS Omega*, *7*(50), 47378–47404. https://doi.org/10.1021/acsomega.2c06906

Schrödinger (2020). *Glide*. 7.1 ed. Schrödinger, LLC.

Schrödinger (2020). *LigPrep* (3.8 ed). Schrödinger, LLC.

Schrödinger (2020). *Maestro* (10.6 ed). Schrödinger LLC.

Schrödinger (2020). *Schrödinger suite*. Schrödinger, LLC.

Sharma, D., Bansal, K. K., Sharma, A., Pathak, M., & Sharma, P. C. (2019). A brief literature and review of patents on thiazole-related derivatives. *Current Bioactive Compounds*, *15*(3), 304–315. https://doi.org/10.2174/1573407214666180827094725

Shen, W., Yu, S., Zhang, J., Jia, W., & Zhu, Q. (2014). Synthesis and biological evaluation of 2-phenoxyacetamide analogues, a novel class of potent and selective monoamine oxidase inhibitors. *Molecules (Basel, Switzerland)*, *19*(11), 18620–18631. https://doi.org/10.3390/molecules191118620

Spilovska, K., Zemek, F., Korabecny, J., Nepovimova, E., Soukup, O., Windisch, M., & Kuca, K. (2016). Adamantane: A lead structure for drugs in clinical practice. *Current Medicinal Chemistry*, *23*(29), 3245–3266. https://doi.org/10.2174/0929867323666160525114026

Stockdale, T. P., & Williams, C. M. (2015). Pharmaceuticals that contain polycyclic hydrocarbon scaffolds. *Chemical Society Reviews*, *44*(21), 7737–7763. https://doi.org/10.1039/c4cs00477a

Sureshkumar, B., Mary, Y. S., Resmi, K., Suma, S., Armaković, S., Armaković, S. J., Van Alsenoy, C., Narayana, B., & Sobhana, D. (2018). Spectroscopic characterization of hydroxyquinoline derivatives with bromine and iodine atoms and theoretical investigation by DFT calculations, MD simulations and molecular docking studies. *Journal of Molecular Structure*, *1167*, 95–106. https://doi.org/10.1016/j.molstruc.2018.04.077

SwissADME Web Tool. Swiss Institute of Bioinformatics.

Turan Yücel, N., Evren, A. E., Kandemir, Ü., & Can, Ö. D. (2022). Antidepressant-like effect of tofisopam in mice: A behavioural, molecular docking and MD simulation study. *Journal of Psychopharmacology (Oxford, England)*, *36*(7), 819–835. https://doi.org/10.1177/02698811221095528

Wanka, L., Iqbal, K., & Schreiner, P. R. (2013). The lipophilic bullet hits the targets: Medicinal chemistry of adamantane derivatives. *Chemical Reviews*, *113*(5), 3516–3604. https://doi.org/10.1021/cr100264t

Wassel, M. M., Ammar, Y. A., Ali, G. A. E., Belal, A., Mehany, A. B., & Ragab, A. (2021). Development of adamantane scaffold containing 1, 3, 4-thiadiazole derivatives: Design, synthesis, anti-proliferative activity and molecular docking study targeting EGFR. *Bioorganic Chemistry*, *110*, 104794. https://doi.org/10.1016/j.bioorg.2021.104794

Wishnok, J. S. (1973). Medicinal properties of adamantane derivatives. *Journal of Chemical Education*, *50*(11), 780–789. https://doi.org/10.1021/ed050p780

World Health Organization. (2021). *Dementia*. WHO.

Yang, X. H., Xiang, L., Li, X., Zhao, T. T., Zhang, H., Zhou, W. P., Wang, X. M., Gong, H. B., & Zhu, H. L. (2012). Synthesis, biological evaluation, and molecular docking studies of 1,3,4-thiadiazol-2-amide derivatives as novel anticancer agents. *Bioorganic & Medicinal Chemistry*, *20*(9), 2789–2795. https://doi.org/10.1016/j.bmc.2012.03.040